SPRINGER BRIEFS IN APPLIED SCIENCES AND TECHNOLOGY · COMPUTATIONAL MECHANICS

Fadzli Mohamed Nazri

Seismic Fragility Assessment for Buildings due to Earthquake Excitation

Springer

SpringerBriefs in Applied Sciences and Technology

Computational Mechanics

More information about this series at http://www.springer.com/series/8886

Fadzli Mohamed Nazri

Seismic Fragility Assessment for Buildings due to Earthquake Excitation

Springer

Fadzli Mohamed Nazri
School of Civil Engineering
Universiti Sains Malaysia
Penang
Malaysia

ISSN 2191-530X ISSN 2191-5318 (electronic)
SpringerBriefs in Applied Sciences and Technology
ISSN 2191-5342 ISSN 2191-5350 (electronic)
SpringerBriefs in Computational Mechanics
ISBN 978-981-10-7124-9 ISBN 978-981-10-7125-6 (eBook)
https://doi.org/10.1007/978-981-10-7125-6

Library of Congress Control Number: 2017958720

Printed on acid-free paper

This Springer imprint is published by Springer Nature
The registered company is Springer Nature Singapore Pte Ltd.
The registered company address is: 152 Beach Road, #21-01/04 Gateway East, Singapore 189721, Singapore

Acknowledgements

I acknowledge the financial support given by the Ministry of Higher Education (MOHE), Malaysia under the Fundamental Research Grant Scheme (6071321)

Contents

Chapter 1
Introduction

Buildings are the major structures that are exposed to damage when earthquakes are triggered. This damage can cause losses including lives and properties. In past earthquake events, such as the Kobe earthquake in 1995, the Aceh earthquake in 2004, and the Kashmir earthquake in 2005, buildings and infrastructures were severely damaged and collapsed (Petal et al. 2008). During these events, the worst damages were often recorded in cities. For example, many people were killed by falling building debris. Therefore, building damage is the main source of seismic losses during earthquakes.

To solve this problem, fragility curves were introduced by researchers to serve as one of main tool in assessing damage and loss during earthquakes. In general, the curves are generated from real earthquake damage data to estimate or predict whether the damage meets or exceeds a certain performance level for a given set of ground motion parameters. In addition, the curves can be applied to predict both pre- and post-earthquake situations. These curves are unique because every building has specific fragility analysis (Hancilar et al. 2014).

Previous studies have reported different methodologies used to develop fragility curves. The upcoming sections provide a comprehensive review of these methodologies and the importance of the fragility curves. These sections focus on the seismic fragility assessment of buildings. Based on prior investigations, these sections present the significant elements that influence building vulnerability; it also aims to briefly discuss the fragility background, introduce the method, and summarize the existing methodologies.

The purpose of this book is to develop fragility curves for regular and irregular frames based on concrete (MRCF) and steel frames (MRSF) for low-, mid-, and high-rise. These frames were designed based on Eurocode 2, Eurocode 3, and Eurocode 8. The pushover analysis (POA) and incremental dynamic analysis (IDA) were performed by using the SAP2000 software. For the dynamic analysis, three sets of near-field (NF) and far-field (FF) ground motion records were used.

F. M. Nazri, *Seismic Fragility Assessment for Buildings due to Earthquake Excitation*, SpringerBriefs in Computational Mechanics,
https://doi.org/10.1007/978-981-10-7125-6_1

References

Hancilar, U., E. Çaktı, M. Erdik, G.E. Franco, and G. Deodatis. 2014. Earthquake vulnerability of school buildings: Probabilistic structural fragility analyses. *Soil Dynamics and Earthquake Engineering* 67: 169–178. https://doi.org/10.1016/j.soildyn.2014.09.005.

Petal, M., R. Green, I. Kelman, R. Shaw and A. Dixit. 2008. Community-Based Construction for Disaster Risk Reduction. *Hazards and the built environment: Attaining built-in resilience*, 191–217.

Chapter 2
Fragility Curves

2.1 Historical Background

Many previous studies, such as those of Kiremidjian (1992), Kumitani and Takada (2004), Akkar et al. (2005), Frankie et al. (2012), Bakhshi and Asadi (2013), Modica and Stafford (2014), Silva et al. (2014), Pragalath et al. (2015), Cutfield et al. (2016), and Joy et al. (2016), present a brief historical background of fragility curve. In these book, fragility curves are defined as the probability of reaching or exceeding a specific damage state under earthquake excitation.

The general equation to develop fragility or conditional probability is expressed by Billah and Alam (2014)

$$\text{Fragility} = P[\text{LS}|\text{IM} = y], \tag{2.1}$$

where,

LS is the limit state or damage state (DS),
IM is the intensity measure (ground motion), and
Y is the realized condition of ground motion IM.

Various equations were derived from previous research (Table 2.1). However, all the equations are based on Eq. (2.1), which is a general equation for generating a fragility curve.

Although most of these studies used different equations to generate their versions of the seismic fragility curves (Table 2.1), most researchers such as Yamaguchi and Yamazaki (2000), Kirçil and Polat (2006), and Ibrahim and El-Shami (2011) used Eq. (2.2) in their studies. This equation is the simplest one in the group. Yamaguchi and Yamazaki (2000) tested Eq. (2.2) for different types of structures and found it to be suitable for use in all structural types. This equation is given below:

F. M. Nazri, *Seismic Fragility Assessment for Buildings due to Earthquake Excitation*, SpringerBriefs in Computational Mechanics,
https://doi.org/10.1007/978-981-10-7125-6_2

Table 2.1 Equations used to develop the fragility curve

Authors	Equation	Parameters	Structure type
Hwang and Jaw (1990)	$P_f = \Phi\left[\frac{-\ln\left(\frac{\bar{\mu}_R}{\bar{\mu}_E}\right)}{\left(\beta_R^2 + \beta_E^2\right)^{1/2}}\right]$	P_f = probability $\Phi[\cdot]$ = standardize normal distribution $\bar{\mu}_R$ = median capacity based on engineering judgment β_R = standard deviation based on engineering judgment $\bar{\mu}_E$ = median from sample β_E = standard deviation from sample	Shear wall
Seya et al. (1993)	$P_f = P_r(R < S) = \int_0^\infty [1 - F_S(r)] f_R(r) dr$	P_f = probability conditional limit state R = structural capacity S = structural response $F_S(\cdot)$ = cumulative probability distribution of S f_R = probability density function of R	MRSF
Singhal and Kiremidjian (1996)	$P_{D\|\mathrm{MMI}}[d\|\mathrm{MMI}] = \int_{S_a} P_{D\|S_a}[d\|S_a] f_{S_a\|\mathrm{MMI}}[S_a\|\mathrm{MMI}] ds_a$	$P_{D\|\mathrm{MMI}}[\mathrm{d}\|\mathrm{MMI}]$ = probability reaching or exceed at specified MMI $P_{D\|S_a}[\mathrm{d}\|S_a]$ = probability reaching or exceed at specified spectral acceleration $f_{S_a\|\mathrm{MMI}}[S_a\|\mathrm{MMI}]$ = conditional probability density function of spectral acceleration at specified MMI	MRCF
Yamaguchi and Yamazaki (2000)	$P(x) = \Phi\left(\frac{\ln X - \lambda}{\varsigma}\right)$	$\Phi[\cdot]$ = standardize normal distribution λ = mean of $\ln x$ ς = standard deviation of $\ln x$	i. Wood-frame ii. Wooden-prefabricated iii. RC iv. Steel-frame v. Light-gauge steel-prefabricated

(continued)

Table 2.1 (continued)

Authors	Equation	Parameters	Structure type
Rosowsky and Ellingwood (2002)	$FR(x) = \Phi\left[\ln\frac{(x/m_R)}{\xi_R}\right]$	$\Phi[\cdot]$ = standardize normal distribution m_R = median capacity x = demand ξ_R = logarithmic standard deviation	Light wood-frame
Kirçil and Polat (2006)	$P(\leq D) = \Phi\left(\frac{\ln X - \lambda}{\varsigma}\right)$	$\Phi[\cdot]$ = standardize normal distribution X = lognormal distributed ground motion index (e.g. S_a, S_d, PGA) λ = mean ς = standard deviation	RC residential building
Lupoi et al. (2006)	$P_f(y_1) = \Pr\left\{ \cup_{j=1 i \in I_{C_j}}^{n_C} \cap C_i(x, \varepsilon_{C_i}) \leq D_i(x \mid y_1) \right\}$	n_C = number of cut-sets I_{C_j} = set of the indices of modes belonging to the jth cut-set	3D RC building
Luco et al. (2011)	For undamaged, $\Pr[\mathrm{IM} > a] = 1 - \Phi\left[\frac{\ln a - \ln m_{\mathrm{IM}}}{\sigma_{\ln \mathrm{IM}}}\right]$ For damaged (post-mainshock), $\Pr[\mathrm{DS} > i] = \int_0^{\infty} \Pr[\mathrm{DS} > i \mid \mathrm{IM} = a] \left\lvert \frac{d \Pr[\mathrm{IM} > a]}{da} \right\rvert da$	$\Pr[\mathrm{IM} > a]$ = fragility for pre-mainshock (undamaged) m_{IM} = median of the IM at each location $\sigma_{\ln \mathrm{IM}}$ = logarithmic standard deviation $\Pr[\mathrm{DS} = i]$ = post-mainshock damage state probabilities	MRCF
Ibrahim and El-Shami (2011)	$P[\mathrm{D/PGA}] = \Phi\left(\frac{\ln(\mathrm{PGA}) - \mu}{\sigma}\right)$	$\Phi[\cdot]$ = standardize normal cumulative distribution μ = mean of natural logarithm σ = standard deviation of natural logarithm	MRCF
Réveillère et al. (2012)	$P(\mathrm{DS} \geq k \mid \mathrm{DS}_{t0} = i, \mathrm{IM}) = \phi\left(\frac{\ln a - \ln \mu_{i,k}}{\beta_{i,k}}\right)$	ϕ = cumulative distributive function of standard normal distribution $\mu_{i,k}$ = median of fragility curve from $DS = i$ to $DS \geq k$ $\beta_{i,k}$ = standard deviation of fragility curve from $DS = i$ to $DS \geq k$	MRCF

(continued)

Table 2.1 (continued)

Authors	Equation	Parameters	Structure type
Jeon et al. (2012)	$P[D_{\mathrm{as}} > C\|\mathrm{IM}_{\mathrm{as}}] = \Phi\left[\frac{\ln(S_{\mathrm{d}}/S_{\mathrm{c}})}{\sqrt{\beta^2_{\mathrm{d}\|\mathrm{IM}_{\mathrm{as}}} + \beta^2_{\mathrm{c}} + \beta^2_{\mathrm{m}}}}\right]$	D_{as} = seismic demand (aftershock) C = structural capacity S_{d} = median of demand $\beta_{\mathrm{d}\|\mathrm{IM}}$ = dispersion of demand S_{c} = median of capacity β_{c} = dispersion of capacity β_{m} = modeling uncertainty (β_{m} = 0.2)	MRCF
Frankie et al. (2012)	$P(\mathrm{Exceedance}_i\|\mathrm{IM}) = \Phi\left[\frac{1}{(\beta_{\mathrm{tot}})_i}\ln\left(\frac{\mathrm{IM}}{\mathrm{LS}_i}\right)\right]$	$\Phi[\cdot]$ = standardize normal cumulative distribution $(\beta_{\mathrm{tot}})_i$ = log SD represent total uncertainty LS_i = threshold value for ith limit state	Unreinforced-masonry (URM)
Polese et al. (2013)	$P\left[\mathrm{col}\|a_{\mathrm{g}}\right] = \Phi\left[\frac{1}{\beta}\cdot\ln\left(\frac{a_{\mathrm{g}}}{\hat{a}_{\mathrm{g}}}\right)\right] = \Phi\left[\frac{1}{\beta}.\ln\left(\frac{a_{\mathrm{g}}}{\mathrm{REC}_{ag}}\right)\right]$	$P\left[\mathrm{col}\|a_{\mathrm{g}}\right]$ = probability of attaining collapse state given peak ground acceleration a_{g} = peak ground acceleration $\Phi[\cdot]$ = standardize normal cumulative distribution β = global value of dispersion REC_{ag} = residual capacity	MRCF
Sudret et al. (2013)	$\mathrm{Frag}(\mathrm{PGA}) = 1 - \Phi\left(\frac{\ln\delta_0 - [\Lambda\ln(\mathrm{PGA}) + \mathrm{B}]}{\zeta}\right)$	PGA = peak ground acceleration $\Phi[\cdot]$ = standardize normal cumulative distribution δ_0 = admissible threshold Λ,B = mean of linear regression in a log-log plot ζ = standard deviation	MRSF

(continued)

Table 2.1 (continued)

Authors	Equation	Parameters	Structure type
Negulescu et al. (2014)	$P_f(\text{ds} \geq \text{ds}_i \mid S) = \Phi\left[\frac{1}{\beta_{\text{tot}}} \cdot \ln\left(\frac{\text{IM}}{\text{IM}_{\text{mi}}}\right)\right]$	$P_f(.)$ = probability of exceeding a particular damage state, ds, for a given intensity level (PGA) Φ = standard cumulative probability function IM_{mi} = median threshold value of earthquake intensity measure β_{tot} = lognormal standard deviation	Masonry building reinforced by tie rods
Barbat et al. (2014)	$P[i/\text{sd}] = \phi\left[\frac{1}{\beta_{\text{ds}_i}} Ln\left(\frac{\text{sd}}{\text{sd}_{\text{ds}_i}}\right)\right]$	sd = spectral displacement sd_{ds_i} = mean value of lognormal distribution which corresponds to damage state threshold β_{ds_i} = standard deviation of natural logarithm of spectral displacement of ds	MRCF
Lee et al. (2014)	$P[C < D \mid SI = x] = 1 - \Phi\left[\frac{\ln(\hat{C}/\hat{D})}{\sqrt{\beta_{D\mid SI}^2 + \beta_c^2 + \beta_m^2}}\right]$	$\Phi[\cdot]$ = standard normal probability integral $\hat{C}$ = median structural capacity $\hat{D}$ = median structural demand $\beta_{D\mid SI}$ = uncertainty in D β_c = uncertainty in C β_m = modeling uncertainty	RC building in Y-shaped and box-shaped
Farsangi et al. (2014)	$P_f = P\left\{\text{U}_{i=1}^{n}\left[\max \frac{u_i}{h_i} \geq LS \mid IM\right]\right\}_t \text{and} \quad 0 < t < t_d$	t_d = duration of the ground motion i = storey level n = number of storey u_i = storey drift h_i = storey height	MRSF
Hancilar et al. (2014)	$P_f(\text{Damage} \geq \text{DS}_i \mid \text{IM}) = \Phi[(1/\beta)\ln(\text{IM}/\mu)]$	Φ = standard cumulative probability function β = log-standard deviation of IM μ = mean of IM	MRCF with shear wall

(continued)

Table 2.1 (continued)

Authors	Equation	Parameters	Structure type
Vona (2014)	$P[d_{Si}\|I_H] = \Phi\left[\frac{1}{\beta_{ds_i}} . \ln\left(\frac{I_H}{\mu_{ds}}\right)\right]$	Φ = standard normal cumulative probability function μ_{ds} = median value of Housner intensity of damage state β_{ds_i} = standard deviation of lognormal of Housner Intensity	MRCF
Banihashemi et al. (2015)	$P(\mathrm{D} > \mathrm{d}_i\|im) = 1 - P(\mathrm{D} \leq \mathrm{d}_i\|im) = 1 - \Phi\left(\frac{\ln\left(\frac{ISD_i}{\overline{ISD}_{\mathrm{im}}}\right)}{\beta_{\mathrm{im}}}\right)$	$\overline{ISD}_{im}$ = medians of ISD distribution β_{im} = deviation lognormal distribution of ISD in each im ISD_i = threshold of different damage state	Steel concentrically braced frames (SCBF)
Wijayanti et al. (2016) and McCrum et al. (2016)	$P[\mathrm{ds}\|S_\mathrm{d}] = \Phi\left[\frac{1}{\beta_{\mathrm{ds}}}\ln\left(\frac{S_\mathrm{d}}{\overline{S}_{\mathrm{d,ds}}}\right)\right]$	S_d = spectral displacement $\overline{S}_{\mathrm{d,ds}}$ = median value of spectral displacement at which the building reaches the threshold of the damage state, ds β_{ds} = standard deviation of the natural logarithm of spectral displacement of damage state, ds Φ = standard normal cumulative distribution function	MRCF
Akhavan et al. (2016)	$F_d(x) = P[D \geq d\|X = x]; d \in \{1, 2, \ldots, N_D\} = \phi\left(\frac{\ln(x/\theta_d)}{\beta_d}\right)$	D = uncertain damage state of particular component d = particular value of D X = uncertain excitation x = particular value of X θ_d = median capacity β_d = standard deviation of natural logarithm of capacity	MRSF

(continued)

Table 2.1 (continued)

Authors	Equation	Parameters	Structure type
Pejovic and Jankovic (2016)	$P\left[\mathrm{DS}_i = \mathrm{IDR} > \mathrm{IDR}^{\mathrm{DS}_i}/\mathrm{IM}\right] = \Phi\left(\frac{\ln \mathrm{IM} - \mu}{\sigma}\right)$	Φ = standard normal cumulative distribution function μ = mean value σ = standard deviation IM = intensity measure IDR = inter-storey drifts	MRCF (high-rise building with core wall structural system)

$$P(x) = \Phi\left(\frac{\ln X - \lambda}{\varsigma}\right) \tag{2.2}$$

where,

$\Phi[\cdot]$ is the standardize normal distribution,
λ is the mean of $\ln x$, and
ς is the standard deviation of $\ln x$.

The fragility curves are established to provide a prediction of potential damage during an earthquake. These curves represent the seismic risk assessment and are used as an indicator to identify the physical damage in the strongest mainshock. Apart from the mainshock, probability aftershock must also be investigated to decide whether or when to permit re-occupancy of a building. The fragility function is also directly used to reduce damage cost and loss of life during a seismic event. Therefore, fragility curves can be used as a decision-making tool for both pre- and post-earthquake situations. Moreover, these curves may help develop future local code provisions.

Two main components in the probabilistic seismic risk assessment have been identified. These components include information about ground motion hazard on the location of structure and fragility knowledge with respect to the intensity of the ground motion. Polese et al. (2014) stated four important factors available for a large database, which include the number of storeys, age of construction, regularity (in plan, elevation, and in-fill), and position of building in the block. Silva et al. (2014) proposed vulnerability curves using the HAZUS tool (HAZUS 1999) for risk assessment. The curves were created specifically for buildings in the US.

2.2 Structural Types

Fragility curves were discussed based on three types of structures, namely, steel, reinforced concrete, and timber. Most studies covered steel and reinforced concrete structures. However, less research has been conducted on timber structure. Many studies developed fragility curves for infrastructures, including those of Shinozuka et al. (2000), Alessandri et al. (2011), Billah and Alam (2014), and Siqueira et al. (2014). However, the fragility curves for buildings are categorized into three types. These types are low-, mid-, and high-rise buildings based on the number of storeys (Table 2.2).

The important factors of vulnerability, which are also available for large databases, include a number of storeys, age of construction, regularity in plan and elevation, infill regularity, and building position in the block (Polese et al. 2014). Thus, classifying buildings is one of the significant factors that must be considered in developing fragility curve. Differences in materials, height, and number of bays also result in different shapes of vulnerability curves. Researchers from different

Table 2.2 Classification of Building by Number of Storeys

Authors	Building Classification		
	Low-rise	Mid-rise	High-rise
	Number of storeys		
Singhal and Kiremidjian (1996), Akkar et al. (2005), Uma et al. (2011)	1–3	4–7	8 and up
Modica and Stafford (2014), Silva et al. (2014a)	1–3	4–6	7 and up
Hancilar et al. (2014)	1–4	5–8	9 and up

countries have developed their respective versions of the curve. Table 2.3 shows the synopsis of fragility analysis performed by several researchers.

2.3 Earthquake Records

Ground motion records play the main role in establishing fragility curves. Selecting an appropriate ground motion and scaling the ground motions are very important in generating this curve. If the ground motion is randomly scaled up to a specific spectral acceleration, S_a, at a period, T, over conservative structural response may occur (Baker et al. 2014).

A few parameters must be considered in selecting ground motion, including event magnitude, peak ground acceleration (PGA), distance between epicenter/source and affected area, and soil type (Nazri and Alexander 2012). In addition, ground motion characteristics must be considered to obtain accurate prediction and to minimize the dispersion of the analytical behavior of buildings. Ground motion characteristics that must be considered include, ground motion intensity, spectral shape, duration, frequency content, near-fault, amplitude, and number of cycles (Ibrahim and El-Shami 2011; Ruiz-García and Negrete-Manriquez 2011; Song et al. 2014).

The selected ground motion must come from previously recorded earthquake events. Ground motion can be selected from certain websites, such as Pacific Earthquake Engineering Research (PEER) NGA database website, Consortium of Organization for Strong Motion Observation System, or K-NET. Silva et al. (2014) list other websites where ground motion records can be obtained, including the European Strong Motion database, the French Accelerometric Network, and the Swiss Earthquake Database.

The suitable number of ground motions depends on the application and structural response prediction. Two types of ground motions are considered as foreshocks: near-field site and far-field site. Researchers discuss a few important factors in selecting ground motion. For far-field site, the important factors include spectral shape over the period range of interest, magnitude, site-to-source distance, and hazard curve at a period, T. Meanwhile, for near-field site, the factors to be

Table 2.3 Summary from Prior Studied

Authors	Highlight	Type of structure	Number of storeys	Number of bays
Hwang and Jaw (1990)	Show a simplified analytical method to develop fragility curve and give an overview about fragility background	Shear wall	5	–
Seya et al. (1993)	Generate fragility curve for steel frame	MRSF	5	3
Holmes (1996)	Show a general step and provide information about fragility curve	–	–	–
Singhal and Kiremidjian (1996)	Use nonlinear history analysis to generate fragility curve	MRCF	2, 5, 12	5
Kircher et al. (1997)	Describe general information about damage, methods to estimate probability on both structural and nonstructural parts developed for the FEMA/NIBS	–	–	–
Yamaguchi and Yamazaki (2000)	Five different types of materials, namely, wood-frame, wooden-fabricated, reinforced concrete (RC), steel-frame, and light-gauge steel-prefabricated, were tested to develop fragility curve based on Kobe earthquake in 1995	Frame	–	–
Lee and Rosowsky (2006)	Develop an appropriate percentage of design snow loads for fragility seismic assessment	Shear wall (wood-frame)	1 and 2	1
Ibrahim and El-Shami (2011)	Discuss the method to develop fragility curve for low- and mid-rise concrete frame	MRCF	3 and 8	3
Uma et al. (2011)	Present the different parameters in the structural model and their impact on vulnerability risk assessment for mainshock and aftershock records. Typical building model in New Zealand and the United States was generic for this study	MRCF	5	–

(continued)

Table 2.3 (continued)

Authors	Highlight	Type of structure	Number of storeys	Number of bays
Jeon et al. (2012)	Evaluate the seismic cumulative damage potential of non-ductile reinforced concrete and their performance and increase the vulnerability after multiple earthquakes	MRCF	3	3
Sudret et al. (2013)	Generate seismic vulnerability curve by using polynomial chaos expansions for steel frame	MRSF	3	3
Goda and Salami (2014)	Study the impact of aftershock on seismic vulnerability of conventional timber frame houses by using a set of real mainshock and aftershock earthquake records	Timber frame	2	1
Kumar et al. (2014)	Propose a simple methodology to assess the probabilistic seismic damage of RC buildings by using nonlinear pushover analysis	MRCF	4	1
Farsangi et al. (2014)	Develop fragility curve and estimate mean annual seismic loss for MRSF in the Middle East area	MRSF	2	2
Ebrahimian et al. (2014)	Develop vulnerability curve and investigate adaptive aftershock risk assessment in terms of daily limit state first-excursion probabilities. In this study, cloud analysis was implemented to develop the fragility curve	MRCF	3	2
Jalayer et al. (2014)	Introduce Bayesian cloud analysis in the fragility curve. Then, this analysis was compared with IDA analysis	MRCF	4	4
Shin et al. (2014)	Propose a methodology to assess the effectiveness of retrofitting with buckling resistance brace	MRCF	5	2
Silva et al. (2014a)	Develop fragility curve for Portuguese RC building	MRCF	–	3

(continued)

Table 2.3 (continued)

Authors	Highlight	Type of structure	Number of storeys	Number of bays
Barbat et al. (2014)	Develop fragility curve and investigate the seismic damage in RC in terms of probability by using Monte Carlo	MRCF	8	6
Silva et al. (2014b)	Estimate the nonlinear response of building by using static and dynamic procedure and investigate the effectiveness of the capacity, fragility, and risk	MRCF	4	3
Hancilar et al. (2014)	Assess and develop a probabilistic curve for a public school in Istanbul	MRCF	4	11
Li et al. (2014)	Study the collapse probability mainshock damage to steel building in aftershock	MRSF	4	4
Aiswarya and Mohan (2014)	Develop fragility curve for flat slab structure and evaluate the seismic vulnerability. Then, determine a method to improve the seismic performance. Unretrofitted and retrofitted structure fragility curves were compared for an office located in Mid-American region	Reinforced concrete flat slab building	5	4
Pragalath et al. (2015)	Propose two techniques to develop seismic fragility curve based on time history analysis and IDA. Both methods have different assumptions and methodologies	MRCF	4	4
Banihashemi et al. (2015)	A newly developed performance-based plastic design (PBPD) methodology was applied to steel special concentric braced frames. Reliability-based assessment based on FEMA 351 indicated that PBPD frames have much higher	Steel concentrically braced frames (SCBF)	6, 9	1

(continued)

Table 2.3 (continued)

Authors	Highlight	Type of structure	Number of storeys	Number of bays
	confidence levels against global collapse than those of corresponding SCBFs designed by current seismic codes and the results are proved by the seismic fragility curves of model frames			
Wijayanti et al. (2016)	Seismic vulnerability assessment for Indonesian reinforced concrete frame building with steel truss roof by using fragility curve	MRCF	4	–
Akhavan et al. (2016)	The seismic response of 2-D MRSF buildings incorporating soft storey is evaluated. The fragility curves for different placement of soft storey in the first, middle, and top floor for 4, 8 and 16-storey buildings are developed and compared	MRSF	4, 8, 16	3
Lin et al. (2017)	Seismic and progressive collapse designs for RC frames are performed independently according to the corresponding design codes. Fragility curves are used to assess the seismic and progressive collapse resistance	MRCF	6	4
McCrum et al. (2016)	Demonstrates the development of fragility curves at different damage states using a detailed mechanical model of an MRCF structure typical of Southern Europe. The mechanical model consists of a complex 3-DFEM of the MRCF structure and is used to define the damage states through pushover analysis	MRCF	3	1

(continued)

Table 2.3 (continued)

Authors	Highlight	Type of structure	Number of storeys	Number of bays
Pejovic and Jankovic (2016)	Seismic fragility assessment of RC high-rise buildings for seismic excitation, typical for Southern Euro-Mediterranean zone. 20-, 30-, and 40-storey RC high-rise buildings with core wall structural system were chosen. Since no probabilistic fragility curves exist for this class of buildings and for this seismic zone, this work partially fills the void in Southern Euro-Mediterranean seismic risk assessment	MRCF (high-rise building with core wall structural system)	20, 30, 40	–

considered include spectral shape and the possible presence of velocity pulses. Table 2.4 presents an overview of recommendations for selecting and scaling ground motion (Haselton et al. 2012).

Apart from obtaining data from the aforementioned databases, ground motion records can also be generated based on the equation. For example, Sudret et al. (2014) generated ground motion records from several equations. The procedure to simulate synthetic ground motion is briefly explained because stimulating synthetic ground motion usually takes too long. In their study, they concluded there are three temporal parameters, three spectral parameters, and a standard Gaussian random vector of size that must be considered to generate a seismic model. Compared with synthetic ground motion, real accelerograms are more widely used as ground motion records and then scaled to cover the range of ground motion level that might occur (Ay and Akkar 2014).

Reasenberg and John (2005) reported that earthquakes occur in clusters, that is, when one earthquake strikes, another earthquake will occur in the nearby locations. According to Uhrhammer (1986), events that only occur in a zone approximately parallel to the fault rupture or surround the main events are considered foreshocks or aftershocks. In an earthquake event, the magnitude can be classified into three terms, namely, foreshock, mainshock, and aftershock. The largest magnitude is called mainshock, whereas the earthquakes that occur before and after the mainshock are called foreshock and aftershock, respectively. However, mainshocks are often redefined as foreshock if a subsequent earthquake in a cluster has a larger magnitude.

Table 2.4 Recommendations for ground motions selecting and scaling modified from Haselton et al. (2012)

Steps for response history analysis	Design/assessment method			
	ASCE7-05	ASCE-10	LATBSDG	PEER TBI
Ground motion selection	–	–	–	–
Number of motions	≥ 7 (or 3) pairs		≥ 7 pairs	
Types of motion	Recorded and/or simulated		Record or simulated (ref to ASCE7-05)	Recorded and/ or simulated
Other	None		Appropriate num. of motion with directivity effects	Directivity if needed
Scaling/ modification of motions to match target spectrum	–	–	–	–
General approach	Scaling (spectral matching not mentioned)		Scaling or spectral matching	
Specific instructions for far-field sites	SRSS is above target 1.17 × target spectrum	SRSS is above target spectrum	SRSS is above target 1.17 × target spectrum (ref to ASCE7-05)	Match records to the target spectrum
Specific instructions for near-field sites	None	Average of FN is above target	None (ref to ASCE7-05)	None
Period range for matching	0.2–1.5 T		0.2–1.5 T (ref to ASCE7-05)	Not specified
Application of ground motions to structural model	–	–	–	–
Far-field sites	Apply only horizontal motions together; no rules for orientation		Orient motions randomly; no need for multiple orientations of GMs	Apply along principle directions if directivity effects dominate
Near-field sites	No rules for orientation	Apply in FN/FP direction if site >5 km from fault	Apply in FN and FP directions	Apply in FN and FP directions if directivity effects dominate

SRSS—Square-Root-Sum-of Squares Spectrum (Ground motion scaling ground motion method)
FN—Fault Normal
FP—Fault Parallel

Most prior research used mainshock records as inputs in their seismic risk assessment. For example, Farsangi et al. (2014) evaluated the seismic vulnerability of moment-resisting steel frame (MRSF) using mainshock ground motion records. They explicitly explained the whole process starting from selecting ground motion records from the PEER website. Seven sets of ground motions were used and the basic characteristics of earthquakes, such as strikes and frequencies, were considered in the selection. Then, the records were scaled to the elastic response spectrum with 5% damping.

Wells and Coppersmith (1994) explained that aftershocks can occur within a few hours to a few days after the mainshock. The fault produces most of the aftershocks when the stress on the mainshock fault changes drastically during the mainshock. These earthquakes can be regarded as aftershocks if they are located within a characteristic distance from the mainshock. This distance usually takes one or two times the length of the fault rupture associated with the mainshock.

In a recent study, aftershock records have been considered in developing the fragility curve. Such aftershock has big potential to induce massive damages and losses. Several aftershock events have been recorded, such as the Chi-Chi earthquake in Taiwan. During this time, a gas station survived the mainshock and then collapsed during the aftershock. Therefore, aftershock events must also be considered in seismic risk assessment.

The methods for selecting and scaling ground motions have been investigated by several researchers (Haselton et al. 2012; Ay and Akkar 2014; Wang and Rosowsky 2014). Haselton et al. (2012) highlighted the best method for selecting and scaling ground motions. They reported that these tasks depend on three types of assessments, namely, intensity-, scenario-, and risk-based (time-based) assessments in ATC-58-1. Of these, the most commonly used is the intensity-based assessment. For selecting and scaling ground motions, proper methods are based on structural response parameter(s) of interest, and either record-to-record variability in structural response or maximum response (collapse response) must be predicted.

Wang and Rosowsky (2014) introduced three new approaches for scaling ground motions. The first approach involves selecting ground motion from the real historic seismic records. The second approach is initially selecting ground motion from the real historic seismic, and then modifying this to satisfy the given site using an amplitude scaling method or spectrum matching method. The third approach involves initially selecting ground motion from seismological model with some information and then generating synthetic ground motions.

Meanwhile, two alternative procedures have been explicitly discussed in the paper of Ay and Akkar (2014). The first proposed procedure is based on the conditional mean spectrum. The second method is based on empirical elastic-to-inelastic conversion factors. In this method, the target inelastic spectral coordinates are initially estimated, and then, the records are scaled to the estimated inelastic target level. In the study of Barbat et al. (2014), 20 acceleration records were selected. Then, these records were scaled to different levels of the peak ground acceleration. Figure 2.1 shows the mean spectrum and spectrum of Eurocode 8 corresponding to the 20 selected ground motions.

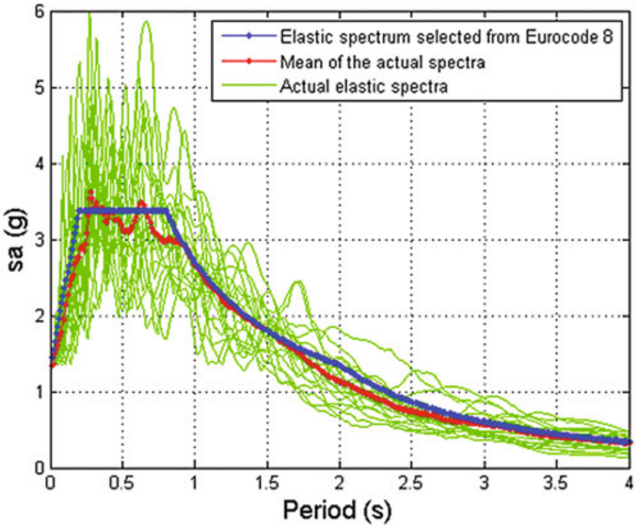

Fig. 2.1 Mean spectrum of selected earthquake events scaled to the spectrum of Eurocode 8 (Barbat et al. 2014)

2.4 Simulation Methods

To develop the fragility curves using the analytical method, a few popular simulation methods need to be applied. The assessment can be categorized into two main groups, namely, NSA and NDA. Some researchers use NSA (Mosalam et al. 1997; Frankie et al. 2012; Polese et al. 2013; Vargas et al. 2013; Garcia 2014; Kumar et al. 2014; Lee et al. 2014; Lee and Moon 2014), nonlinear time history analysis (NTHA) (Aiswarya and Mohan 2014; Farsangi et al. 2014; Wang and Rosowsky 2014), and incremental dynamic analysis (IDA) (Luco et al. 2011; Ryu et al. 2011; Uma et al. 2011; Bakhshi and Asadi 2013; Charalambos et al. 2014; Raghunandan et al. 2014; Sudret et al. 2014). The next sections will present a review of different simulation methods employed to develop fragility curve. Some software are available to perform this analysis. Table 2.5 shows some of such software used by researchers.

2.4.1 Nonlinear Static Analysis

Nonlinear static analysis or pushover analysis (POA) is one of the methods used to develop fragility seismic curves. Polese et al. (2013) initially evaluated the appropriateness of POA in damage analysis, from which they developed the

Table 2.5 Available software used by researchers

Authors	Structural type	Software
Seya et al. (1993)	MRSF	DRAIN-2D
Singhal and Kiremidjian (1996)	MRCF	DRAIN-2DX
Akkar et al. (2005), Hancilar et al. (2014)	MRCF	SAP2000
Kirçil and Polat (2006)	RC residential building (3D)	IDARC
Lee and Rosowsky (2006)	Wood-frame (shear wall)	SAW and CASHEW
Lupoi et al. (2006), Ryu et al. (2011), Uma et al. (2011), Jeon et al. (2012), Réveillère et al. (2012), Shome et al. (2014), Silva et al. (2014), Hancilar et al. (2014)	MRCF (2D and 3D)	OpenSees
Ibrahim and El-Shami (2011)	MRCF	SeismoStruct
Ruiz-García and Negrete-Manriquez (2011)	MRSF	Ruaumoko
Bakhshi and Asadi (2013)	MRSF	IDARCV7.0
Sudret et al. (2013), Li et al. (2014), Farsangi et al. (2014)	MRSF	OpenSees
Negulescu et al. (2014)	Masonry building reinforced by tie-rods	TREMURI
Goda and Salami (2014), Shome et al. (2014)	Wood-frame	SAWS for wood structure
Garcia (2014)	MRSF	SAP2000
Banihashemi et al. (2015)	Steel concentrically braced frames (SCBF)	OpenSees
Wijayanti et al. (2016)	MRCF	HAZUS
Akhavan et al. (2016)	MRSF	HAZUS-MH
McCrum et al. (2016)	MRCF	ABAQUS
Pejovic and Jankovic (2016)	MRCF	PERFORM-3D

fragility curve. They conducted the analysis of intact structures and damaged buildings, resulting in a capacity curve. Moreover, Kumar et al. (2014) mentioned that capacity curves can represent mean or mean plus/minus with one/two/three times the standard deviation of capacity curves. From these capacity curves, the results can be compared with those of the Performance-Based Seismic Design (PBSD) in generating fragility curve.

2.4.2 Nonlinear Dynamic Analysis

It is important to choose a nonlinear analysis tool while considering its limitation. Such a toll can provide an accurate investigation and stable NTHA of the structure

(Farsangi et al. 2014). The NDA or NTHA method considers geometric nonlinearity and material inelasticity in predicting the displacement behavior and collapse load. In addition, this method requires a ground motion. A suitable set of ground motions is needed to ensure the accuracy of the fragility curves. However, the suitability of the set of ground motion is a significant issue (Billah and Alam 2014).

Vona (2014) investigated fragility curves based on different methods of analysis, namely, POA and NDA. According to this study, it has been shown that NDA is the most accurate method for investigating the moment resisting concrete frames (MRCF) performance. This method can consider the real characteristics as inputs, from which it can evaluate structural response.

In addition, Silva et al. (2014) reported that NDA applies acceleration time history analysis, which then leads to accurate results. However, they found that NDA is time-consuming. Thus, they introduced several methods, such as capacity spectrum method, displacement coefficient method (DCM) and N2 method, as alternatives. In conclusion, they suggested use of NSA as a valid alternative for obtaining results rapidly and accurately.

Billah and Alam (2014) argued that NTHA requires a large number of ground motions, making the computational analyses expensive. Thus, they introduced IDA to replace NTHA. They mentioned that Luco and Cornell (1998) first developed this method, which used to be a part of NTHA (both are found to be similar). However, ground motion in IDA is scaled in increments, thereby, resulting in a different performance depending on the intensity level.

The aforementioned assumption is supported by Colapietro et al. (2014), who argued that IDA is an extension method of NTHA or NDA. This method properly estimates the performance of structure under seismic load through certain sets of ground motion records and scales the ground motion records to obtain the response curve. Upon comparing the results of IDA and POA methods, they concluded that POA shows good correlation with IDA. However, the POA is more conservative than the latter, especially in predicting higher mode effects in the post-elastic range, which considers irregular buildings with limited capabilities of fixed load distributions. IDA can be used to investigate complexities and extreme irregularities of analyzed buildings. Given that the reliability of an analysis is related to the level of knowledge, the authors suggest that destructive and non-destructive tests should be performed to obtain more realistic estimations of seismic variability.

Ryu et al. (2011) performed IDA analysis to develop fragility curves using a typical New Zealand 5-storey MRCF. This paper shows the process application of IDA. The first step is choosing the mainshock and aftershock ground motion records. In this study, 30 sets of ground motions were selected. Then, IDA was performed in sequence using the mainshock and aftershock records. The fragility curves were finally computed from the analysis results. Meanwhile, other authors such as Ibrahim and El-Shami (2011) and Shome et al. (2014) used IDA as an input to develop seismic vulnerability curve.

2.5 Performance-Based Seismic Design (PBSD)

Manafpour and Moghaddam (2014) reviewed the advantages and disadvantages of probabilistic PBSD by considering all its constraints and limitations. They found that PBSD provides a quantitative measure for structural damage by considering specific earthquake level.

PBSD can be used for several purposes to:

(i) obtain better performance results for new buildings,
(ii) determine performance in accordance with code provisions with the subsequent development of the required adjustment,
(iii) enhance current provisions to obtain good designs, and
(iv) provide an efficient retrofit design procedure.

These authors argue that the performance of seismic assessment depends on three factors, namely, the ground motion types, resisting lateral load, and height of the buildings. Meanwhile, PBSD can be determined based on the percentage of maximum interstorey drift. Interstorey drift was used because this factor can be easily measured during the analysis and provides a clear result. Interstorey drift can be classified into five categories, namely, operational phase (OP), immediate occupancy (IO), damage control (DC), life safety (LS), and collapse prevention (CP) (Ibrahim and El-Shami 2011). By contrast, other authors, such as Uma et al. (2011), classified interstorey drift into slight, moderate, extensive, complete, and collapse. Table 2.6 summarizes each limit state with the percentage of maximum drift.

Table 2.6 Summary of performance level and percentage of maximum drift

Authors	Performance level (%)				
	OP	IO	DC	LS	CP
Rosowsky and Ellingwood (2002)	0.5	1.0	–	<5.0	>5.0
Lee and Rosowsky (2006)	–	1.0	–	2.0	3.0
Uma et al. (2011) for New Zealand model	0.7	0.14	2.0	2.6	3.9
Uma et al. (2011) for US model	0.5	0.14	3.0	3.5	5.3
Ibrahim and El-Shami (2011)	0.5	1.0	1.5	2.0	2.5
Ruiz-García and Negrete-Manriquez (2011)	–	0.7	–	2.5	5.0
Li et al. (2014)	–	0.7	–	2.5	5.0
Silva et al. (2014)	0.05	0.3	1.15	2.8	>4.36
Shin et al. (2014)	–	1.0	2.0	4.0	>4.0
Aiswarya and Mohan (2014)	–	1.0	–	2.0	4.0
Negulescu et al. (2014)	0.0031	0.004	0.0066	0.0119	0.0207
Pragalath et al. (2015)	–	1.0	–	2.0	4.0

Ibrahim and El-Shami (2011) defined each limit state. The building is at an OP state when it is suitable for normal use with least or no damage. At an IO state, the building has minimal or no structural damage and minor non-structural damage. The LS state is when the building appears to have structural and non-structural damages, which require repairs before re-occupancy. At a CP state, the structural and non-structural parts of the building are prevented from collapsing. Meanwhile, Silva et al. (2014) define drift as slightly damaged when 50% of maximum base shear capacity is achieved. The drift is in a moderate state when 75% of maximum base shear capacity is achieved and is in a collapsed state when the ultimate drift taken from the pushover curve is decreased by 20 or 75% (whichever comes first).

A few guidelines, such as FEMA-356 and ATC-40, have been established to improve building performance (Charalambos et al. 2014). The PEER center methodology has been proposed to gain an overall assessment of building performance at any intensity level and limit state by integrating data related to seismic hazard and damage from the structural analysis and loss.

2.6 Methods to Develop Fragility Curves

The fragility curves are an important tool to assess seismic risk. Every building or structure has its own fragility curve. This seismic fragility curves can be used as follows:

(i) for assessing potential effects and risks, including functional and loss in economic and lives,
(ii) for emergency or disaster response planning, and
(iii) for risk mitigation efforts (retrofitting).

Based on the literature review, four methods to develop fragility curves can be identified, namely: (i) expert-based or judgmental, (ii) empirical, (iii) analytical, and (iv) hybrid. Billah and Alam (2014) present the advantages and disadvantages of each method to develop fragility curves (Table 2.7).

Figure 2.2 shows the flowchart of the commonly used methodologies to develop fragility curve. Among these methods, analytical fragility curves are the most widely used (Lee and Moon 2014). All of these methods will be explained in detail in the subsequent sections.

2.6.1 Expert-Based Method

Expert-based method or heuristic method is the oldest and simplest one among those mentioned above. Here, the damage distribution of a building subjected to

Table 2.7 Advantages and disadvantages of each method (Billah and Alam 2014)

Method	Advantages	Disadvantages
Expert based	Simple method All factors may be included	Very subjective Totally dependent on the panel expertise Not so accurate
Empirical	Show the actual vulnerability Represent a realistic picture	Lack of data Inconsistency in damage observation
Analytical	Less biased All types of uncertainties are considering	Costly computation Takes too long
Hybrid	Consider post-earthquake data Computational effort can be reduced	Require multiple data because of combination of experimental and analytical High inconsistency in demand model

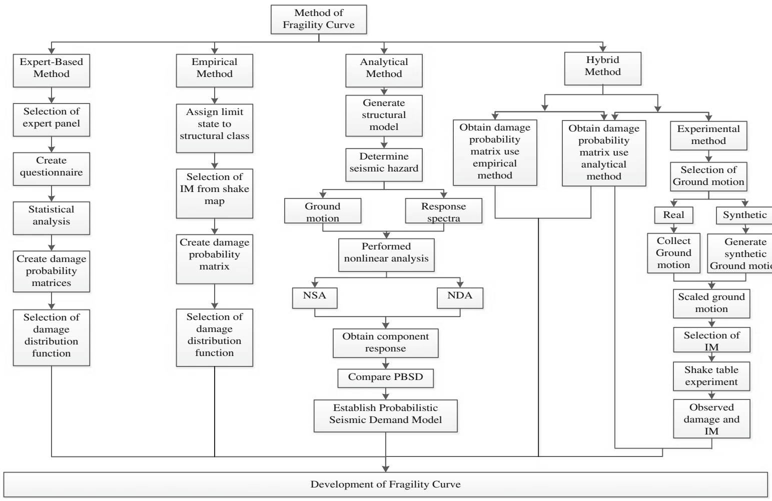

Fig. 2.2 Methods and steps to develop the fragility curve

different earthquake intensities is estimated by civil engineers, who are deemed experts in the field of earthquake engineering.

Fragility estimates are found from the probability distribution of the damage state at each intensity level. ATC-13 and ATC-40 reports have been specifically prescribed for methods based on expert opinions (Farsangi et al. 2014).

Billah and Alam (2014) added information about ATC-13; in their report, the damage matrices and risks for typical infrastructures in California were documented by 42 expert opinions. In accordance with their responses, the probability damage matrix was developed based on the modified Mercalli intensity value. Expert opinion is the only source for this method. Thus, this method depends on the use of questionnaires, the experiences of experts, and the number of experts consulted. In general, their judgments or opinions may contain uncertainties and may be less accurate, thus affecting the quality of the result.

2.6.2 Empirical Method

The fragility curve developed by this empirical method is based on previous earthquake events. For example, the fragility curves were developed using damage data from the 1995 Kobe earthquake. The curves were established by assuming the measurement error; the intensity measure is insignificant.

Ioannou et al. (2015) used this approach to generate seismic curves for a reinforced concrete frame. The whole process is clearly explained in their paper. They initially determined the seismic damage by modeling two uncertainties, after which they simulated ground motions. Finally, they used Eq. (2.1) to generate the fragility curves based on the empirical method. The resulting equation is given by Eqs. (2.3) and (2.4).

$$Y_{jk}|\mathrm{IM}_{'\mathrm{true}'} = \mathrm{iml}_{'\mathrm{true}' \cdot k} \sim \binom{n}{y_{jk}} {\mu_{jk}}^{y_{jk}} \left[1 - \mu_{jk}\right]^{\eta - y_{jk}} \tag{2.3}$$

where,

$$\mu_{jk} = P(\mathrm{DS} \geq \mathrm{ds}_i|\mathrm{iml}_{'\mathrm{true}' \cdot k}) = \Phi\left(\frac{\ln(\mathrm{iml}_{'\mathrm{true}' \cdot k}) - \lambda_k}{\zeta_k}\right) \tag{2.4}$$

λ_k is the lognormal mean and

ζ_k is the lognormal standard deviation for realization k [estimated from Eq. (2.3)].

In conclusion, they argued that variability ground motion may result in flat curves and wide confidence level. A very dense network of ground motion in the recorded data is required to reduce the uncertainty in the empirical fragility curves (Cunha et al. 2014).

2.6.3 Analytical Method

The fragility curves can be generated using this technique even if damage data are insufficient. The analytical method is the most popular method in developing vulnerability seismic curves because this approach has less bias. This approach is developed using simulated data from time history analysis of structural model for real or synthetic ground motions (Farsangi et al. 2014).

2.6.4 Hybrid Method

Kammula et al. (2014) reported that the weakness of the analytical method is its requirement to produce a realistic model, that is, if the model is improperly designed or unrealistic, then it may result in inaccurate estimation that can affect the fragility curve. Considering this problem, some researchers introduced a hybrid approach to improve the analytical method.

The hybrid fragility curves are derived by combining experimental and analytical methods. According to Kappos et al. (2006), the hybrid approach is a calibrated empirical and analytical method, which is conducted by integrating numerical method to solve a numerical structural model equation. This equation considers the analytical and physical components of a structural system.

By considering both the analytical and physical components, the effect of earthquakes on the structures (e.g., buildings and bridges) can be determined. They showed the step-by-step development of fragility curves for a 6-storey structure with telescoping self-centering energy dissipative bracing systems based on hybrid approach. The establishment of the framework, formulation model, ground motion, and result simulation of the hybrid method was briefly discussed in their paper.

Billah and Alam (2014) reported that the hybrid approach involves large aleatory and epistemic uncertainties, which are important elements in generating a probabilistic curve. According to Cunha et al. (2014), aleatory uncertainties include material properties and wind loads that cannot be reduced by collecting additional information. Meanwhile, epistemic uncertainties include the lack of knowledge and incorrect modeling. However, these uncertainties can be reduced by obtaining more information.

References

Aiswarya, S., and N. Mohan. 2014. Vulnerability analysis by the Development of Fragility Curves. *IOSR Journal of Mechanical and Civil Engineering*, 33–40.

Akhavan, N., Sh. Tavousi Tafreshi, and A. Ghasemi. 2016. Fragility Assessment for vertically Irregular Buildings with Soft Storey. *International Journal of Civil, Environmental, Structural, Construction and Architectural Engineering*, at Barcelona, Spain 10 (10): 1274–1282.

Akkar, S., H. Sucuoğlu, and A. Yakut. 2005. Displacement-based fragility functions for low-and mid-rise ordinary concrete buildings. *Earthquake Spectra* 21 (4): 901–927. https://doi.org/10.1193/1.2084232.

Alessandri, S., R. Giannini, and F. Paolacci. 2011. A New Method for Probabilistic Aftershock Risk Evaluation of Damaged Bridge. In COMPDYN 2011-III ECCOMAS Thematic Conference on Computational Methods in Structural Dynamics and Earthquake Engineering.

Ay, B. Ö., and S. Akkar. 2014. Evaluation of a Recently Proposed Record Selection and Scaling Procedure for Low-Rise to Mid-Rise Reinforced Concrete Buildings and Its Use for Probabilistic Risk Assessment Studies. *Earthquake Engineering & Structural Dynamics* 43: 889–908. https://doi.org/10.1002/eqe.2378.

Baker, J.W., T. Lin, and C.B. Haselton. 2014. Ground Motion Selection for Performance-Based Engineering: Effect of Target Spectrum and Conditioning Period. *Performance-based Seismic Engineering: Vision for an Earthquake Resilient Society* 32: 423.

Bakhshi, A., and P. Asadi. 2013. Probabilistic Evaluation of Seismic Design Parameters of Rc Frames Based on Fragility Curves. *Scientia Iranica* 20: 231–241. https://doi.org/10.1016/j.scient.2012.11.012.

Banihashemi, A.R., and M.H.R. Tavakoli. 2015. Performance-based plastic design method for steel concentric braced frames. *International Journal of Advanced Structural Engineering (IJASE)* 7 (3): 281–293. https://doi.org/10.1007/s40091-015-0099-0.

Barbat, A. H., H. Alejandro, Y.F. Vargas, L.G. Pujades, and J.E. Hurtado. 2012. Probabilistic assessment of the seismic damage in reinforced concrete buildings. A: International symposium computational civil engineering. In Proceedings of the 10th International Symposium Computational Civil Engineering, Iasi, Romania, May 25th, 2012. Iasi, Societatea Academica, 2012, 43–61.

Billah, A., and M. Alam. 2014. Seismic Fragility Assessment of Highway Bridges: A State-of-the-Art Review. *Structure and Infrastructure Engineering*, 1–29. https://doi.org/10.1080/15732479.2014.912243.

Charalambos, G., V. Dimitrios, and C. Symeon. 2014. Damage Assessment, Cost Estimating, and Scheduling for Post-Earthquake Building Rehabilitation Using BIM. Computing in Civil and Building Engineering (2014). ASCE, 398–405. https://doi.org/10.1061/9780784413616.050#sthash.LO9sx4WX.dpuf.

Colapietro, D., A. Netti, A. Fiore, F. Fatiguso, and G.C. Marano. 2014. On the Definition of Seismic Recovery Interventions in Rc Buildings by Non-Linear Static and Incremental Dynamic Analyses. *International Journal of Mechanics* 8: 216–222.

Cunha, A., E. Caetano, P. Ribeiro, and G. Müller. 2014. Earthquake Risk Analysis of Structures. In 9th International Conference on Structural Dynamic, EURODYN 2014, Porto, Portugal.

Cutfield, M., K. Ryan, and Q. Ma. 2016. Comparative life cycle analysis of conventional and base-isolated buildings. *Earthquake Spectra* 32 (1): 323–343.

Ebrahimian, H., F. Jalayer, D. Asprone, A.M. Lombardi, W. Marzocchi, A. Prota, and G. Manfredi. 2014. A Performance-Based Framework for Adaptive Seismic Aftershock Risk Assessment. *Earthquake Engineering and Structural Dynamics* 43: 2179–2197. https://doi.org/10.1002/eqe.2444.

Farsangi, E.N., F.H. Rezvani, M. Talebi, and S.A. Hashemi. 2014. Seismic Risk Analysis of Steel-MRFs by Means of Fragility Curves in High Seismic Zones. *Advances in Structural Engineering* 17 (9): 1227–1240.

Frankie, T.M., B. Gencturk, and A.S. Elnashai. 2012. Simulation-based fragility relationships for unreinforced masonry buildings. *Journal of Structural Engineering* 139 (3): 400–410.

Garcia, H.A. 2014. Modal pushover analysis for seismic vulnerability analysis.

Goda, K., and M.R. Salami. 2014. Inelastic Seismic Demand Estimation of Wood-Frame Houses Subjected to Mainshock-Aftershock Sequences. *Bulletin of Earthquake Engineering* 12: 855–874. https://doi.org/10.1007/s10518-013-9534-4.

Hancilar, U., E. Çaktı, M. Erdik, G.E. Franco, and G. Deodatis. 2014. Earthquake vulnerability of school buildings: Probabilistic structural fragility analyses. *Soil Dynamics and Earthquake Engineering* 67: 169–178.

Haselton, C., A. Whittaker, A. Hortacsu, J. Baker, J. Bray, and D. Grant. 2012. Selecting and scaling earthquake ground motions for performing response-history analyses. Proceedings of the 15th World Conference on Earthquake Engineering.

HAZUS. 1999. *Earthquake Loss Estimation*. Washington, DC: Technical Manual, National Institute of Building Sciences.

Holmes, W.T. 1996. Seismic Evaluation of Existing Buildings: State of the Practice. In Proceedings of the 11th World Conference on Earthquake Engineering, Acapulco, Mexico.

Hwang, H.H., and J.-W. Jaw. 1990. Probabilistic Damage Analysis of Structures. *Journal of Structural Engineering* 116: 1992–2007. https://doi.org/10.1061/(ASCE)0733-9445(1990)116:7(1992)#sthash.gpYo9OKl.dpuf.

Ibrahim, Y.E., and M.M. El-Shami. 2011. Seismic Fragility Curves for Mid-Rise Reinforced Concrete Frames in Kingdom of Saudi Arabia. *The IES Journal Part A: Civil & Structural Engineering* 4, no. 4: 213–223.

Ioannou, I., J. Douglas, and T. Rossetto. 2015. Assessing the impact of ground-motion variability and uncertainty on empirical fragility curves. *Soil Dynamics and Earthquake Engineering* 69: 83–92. https://doi.org/10.1016/j.soildyn.2014.10.024.

Jalayer, F., R. De Risi, and G. Manfredi. 2014. Bayesian Cloud Analysis: Efficient Structural Fragility Assessment Using Linear Regression. *Bulletin of Earthquake Engineering*, 1–21. https://doi.org/10.1007/s10518-014-9692-z.

Jeon, J., R. DesRoches, I. Brilakis, and L. Lowes. 2012. Aftershock fragility curves for damaged non-ductile reinforced concrete buildings. In 15th World Conf. on Earthquake Engineering, International Association for Earthquake Engineering (IAEE), Tokyo, Japan.

Joy, R., C.K. Prasad, and V. Thampan. 2016. Development of Analytical Fragility Curve—A Review, 713–716.

Kammula, V., J. Erochko, O.S. Kwon, and C. Christopoulos. 2014. Application of Hybrid-Simulation to Fragility Assessment of the Telescoping Self-Centering Energy Dissipative Bracing System. *Earthquake Engineering and Structural Dynamics* 43: 811–830. https://doi.org/10.1002/eqe.2374.

Kappos, A.J., G. Panagopoulos, C. Panagiotopoulos, and G. Penelis. 2006. A Hybrid Method for the Vulnerability Assessment of R/C and Urm Buildings. *Bulletin of Earthquake Engineering* 4: 391–413. https://doi.org/10.1007/s10518-006-9023-0.

Kircher, C. A., A.A. Nassar, O. Kustu, and W.T. Holmes. 1997. Development of Building Damage Functions for Earthquake Loss Estimation. *Earthquake Spectra* 13: 663–682. https://doi.org/10.1193/1.1585974.

Kirçil, M.S., and Z. Polat. 2006. Fragility Analysis of Mid-Rise R/C Frame Buildings. *Engineering Structures* 28: 1335–1345. https://doi.org/10.1016/j.engstruct.2006.01.004.

Kiremidjian, A.S. 1992. Methods for Regional Damage Estimation. In Proceedings of the 10th World's Conference on Earthquake Engineering. Madrid, Spain, 19–24.

Kumar, C.R., K.B. Narayan, and D.V. Reddy. 2014. Probabilstic Seismic Risk Evaluation Of RC Buildings. *International Journal of Research in Engineering and Technology* 03 (01): 484–495.

Kumitani, S., and T. Takada. 2004. Probabilistic Assessment of Buildings Damage Considering Aftershocks of Earthquakes. In 13th World Conference on Earthquake Engineering, Vancouver, BC, Canada.

Lee, Y., and D. Moon. 2014. A new methodology of the development of seismic fragility curves. *Smart Structures and Systems* 14 (5): 847–867.

Lee, J., S. Han, and J. Kim. 2014. Seismic Performance Evaluation of Apartment Buildings with Central Core. *International Journal of High-Rise Buildings* 3 (1): 9–19.

Lee, K.H., and D.V. Rosowsky. 2006. Fragility Analysis of Woodframe Buildings Considering Combined Snow and Earthquake Loading. *Structural Safety* 28: 289–303. https://doi.org/10.1016/j.strusafe.2005.08.002.

Li, Y., R. Song, and J.W. Van De Lindt. 2014. Collapse Fragility of Steel Structures Subjected to Earthquake Mainshock-Aftershock Sequences. Journal of Structural Engineering.

Lin, K., Y. Li, X. Lu, and H. Guan. 2017. Effects of seismic and progressive collapse designs on the vulnerability of RC frame structures. *Journal of Performance of Constructed Facilities* 31 (1): 04016079.

Luco, N., and C.A. Cornell. 1998. Effects of random connection fractures on the demands and reliability for a 3-story pre-Northridge SMRF structure. In Proceedings of the 6th US national conference on earthquake engineering, vol. 244, 1–12.

Luco, N., M. Gerstenberger, S. Uma, H. Ryu, A. Liel, and M. Raghunandan. 2011. A Methodology for Post-Mainshock Probabilistic Assessment of Building Collapse Risk. In Ninth Pacific Conference on Earthquake Engineering, Auckland, New Zealand.

Lupoi, G., P. Franchin, A. Lupoi, and P.E. Pinto. 2006. Seismic Fragility Analysis of Structural Systems. *Journal of Engineering Mechanics* 132: 385–395. https://doi.org/10.1061/(ASCE)0733-9399(2006)132:4(385)#sthash.NktwK9pH.dpuf.

Manafpour, A.R., and P.K. Moghaddam. 2014. Probabilistic Approach to Performance-Based Seismic Design of RC Frames. Vulnerability, Uncertainty, and Risk: Quantification, Mitigation, and Management, ASCE, 1736–1745.

McCrum, D.P., G. Amato, and R. Suhail. 2016. Development of Seismic Fragility Functions for a Moment Resisting 44: 42–51. https://doi.org/10.2174/1874836801610010042.

Modica, A., and P.J. Stafford. 2014. Vector Fragility Surfaces for Reinforced Concrete Frames in Europe. *Bulletin of Earthquake Engineering*, 1–29. https://doi.org/10.1007/s10518-013-9571-z.

Mosalam, K. M., G. Ayala, R.N. White, and C. Roth. 1997. Seismic Fragility of Lrc Frames with and without Masonry Infill Walls. *Journal of Earthquake Engineering* 1: 693–720. https://doi.org/10.1080/13632469708962384.

Nazri, F., and N. Alexander. 2012. Predicting the Collapse Potential of Structures in Earthquake. University of Bristol.

Negulescu, C., T. Ulrich, A. Baills, and D. Seyedi. 2014. Fragility Curves for Masonry Structures Submitted to Permanent Ground Displacements and Earthquakes. *Natural Hazards*, 1–14. https://doi.org/10.1007/s11069-014-1253-x.

Pejovic, J., and S. Jankovic, 2016. Seismic fragility assessment for reinforced concrete high-rise buildings in Southern Euro-Mediterranean zone. *Bulletin of Earthquake Engineering* 14 (1): 185–212.

Polese, M., M. Di Ludovico, A. Prota, and G. Manfredi. 2013. Damage-Dependent Vulnerability Curves for Existing Buildings. *Earthquake Engineering and Structural Dynamics* 42: 853–870. https://doi.org/10.1002/eqe.2249.

Polese, M., M. Marcolini, G. Zuccaro, F. Cacace. 2014. Mechanism based assessment of damage-dependent fragility curves for RC building classes. *Bulletin of Earthquake Engineering*, 1–23. https://doi.org/10.1007/s10518-014-9663-4.

Pragalath, D.H., R. Davis, and P. Sarkar. 2015. Reliability Evaluation of Rc Frame by Two Major Fragility Analysis Methods. *Asian Journal of Civil Engineering (BHRC)* 16: 47–66.

Raghunandan, M., A.B. Liel, and N. Luco. 2014. Aftershock collapse vulnerability assessment of reinforced concrete frame structures. *Earthquake Engineering & Structural Dynamics*. https://doi.org/10.1002/eqe.2478.

Reasenberg, A.P., and M.L. John. 2005. Some Facts About Aftershocks to Large Earthquakes in California. USGS open file report, 96–266.

Réveillère, A., P. Gehl, D. Seyedi, and H. Modaressi. 2012. Development of Seismic Fragility Curves for Mainshock-Damaged Reinforced-Concrete Structures. In Proceedings of the 15th World Conference on Earthquake Engineering.

Rosowsky, D.V., and B.R. Ellingwood. 2002. Performance-based engineering of wood frame housing: Fragility analysis methodology. *Journal of Structural Engineering* 128 (1): 32–38.

Ruiz-García, J., and J.C. Negrete-Manriquez. 2011. Evaluation of Drift Demands in Existing Steel Frames under as-Recorded Far-Field and near-Fault Mainshock–Aftershock Seismic Sequences. *Engineering Structures* 33: 621–634. https://doi.org/10.1016/j.engstruct.2010.11.021.

Ryu, H., N. Luco, S. Uma, and A. Liel. 2011. Developing Fragilities for Mainshock-Damaged Structures through Incremental Dynamic Analysis. In Ninth Pacific Conference on Earthquake Engineering, Auckland, New Zealand.

Seya, H., M.E. Talbott, and H.H. Hwang. 1993. Probabilistic Seismic Analysis of a Steel Frame Structure. *Probabilistic Engineering Mechanics* 8: 127–136. https://doi.org/10.1016/0266-8920(93)90006-H.

Shin, J., J. Kim, and K. Lee. 2014. Seismic Assessment of Damaged Piloti-Type Rc Building Subjected to Successive Earthquakes. *Earthquake Engineering and Structural Dynamics*. https://doi.org/10.1002/eqe.2412.

Shinozuka, M., M.Q. Feng, H.-K. Kim, and S.-H. Kim. 2000. Nonlinear static procedure for fragility curve development. *Journal of Engineering Mechanics* 126 (12): 1287–1295.

Shome, N., N. Luco, M.C. Gerstenberger, O.S. Boyd, N.E.H. Field, A.B. Liel, and J.W. van de Lindt. 2014. Aftershock Risks Such as Those Demonstrated by the Recent Events in New Zealand and Japan.

Silva, V., H. Crowley, H. Varum, R. Pinho, and L. Sousa. 2014a. Development of a Fragility Model for Moment-frame RC buildings in Portugal. 2nd ICVRAM, Liverpool, UK.

Silva, V., H. Crowley, H. Varum, R. Pinho, and R. Sousa. 2014b. Evaluation of Analytical Methodologies Used to Derive Vulnerability Functions. *Earthquake Engineering and Structural Dynamics* 43: 181–204. https://doi.org/10.1002/eqe.2337.

Singhal, A., and A.S. Kiremidjian. 1996. Method for Probabilistic Evaluation of Seismic Structural Damage. *Journal of Structural Engineering-ASCE* 122: 1459–1467. https://doi.org/10.1061/(ASCE)0733-9445(1996)122:12(1459)#sthash.0ACtmOb5.dpuf.

Siqueira, G.H., A.S. Sanda, P. Paultre, and J.E. Padgett. 2014. Fragility Curves for Isolated Bridges in Eastern Canada Using Experimental Results. *Engineering Structures* 74: 311–324. https://doi.org/10.1016/j.engstruct.2014.04.053.

Song, R., Y. Li, and J.W. van de Lindt. 2014. Impact of Earthquake Ground Motion Characteristics on Collapse Risk of Post-Mainshock Buildings Considering Aftershocks. *Engineering Structures* 81: 349–361. https://doi.org/10.1016/j.engstruct.2014.09.047.

Sudret, B., C. Mai, and V. Mai. 2013. Computing seismic fragility curves using polynomial chaos expansions, Eidgenössische Technische Hochschule Zürich.

Sudret, B., C. Mai, and K. Konakli. 2014. Computing seismic fragility curves using non-parametric representations. arXiv:1403.5481.

Uhrhammer, R.A. 1986. Characteristics of Northern and Central California Sesimicity. *Earthquake Notes* 21.

Uma, S., H. Ryu, N. Luco, A. Liel, and M. Raghunandan. 2011. Comparison of Main-Shock and Aftershock Fragility Curves Developed for New Zealand and Us Buildings. In Proceedings of the ninth pacific conference on earthquake engineering structure building and Earthquake-Resilient Society, Auckland, New Zealand, 14–16.

Vargas, Y.F., L.G. Pujades, A.H. Barbat, and J.E. Hurtado. 2013. Capacity, Fragility and Damage in Reinforced Concrete Buildings: A Probabilistic Approach. *Bulletin of Earthquake Engineering* 11: 2007–2032. https://doi.org/10.1007/s10518-013-9468-x.

Vona, M. 2014. Fragility Curves of Existing Rc Buildings Based on Specific Structural Performance Levels. *Open Journal of Civil Engineering*. https://doi.org/10.4236/ojce.2014.42011.

Wang, Y., and D.V. Rosowsky. 2014. Effects of Earthquake Ground Motion Selection and Scaling Method on Performance-Based Engineering of Wood-Frame Structures. *Journal of Structural Engineering*. https://doi.org/10.1061/(ASCE)ST.1943–541X.0001016#sthash.RitmuRN9.dpuf.

Wells, L.A., and K.J. Coppersmith. 1994. New empirical relationships among magnitude, rupture length, rupture width, rupture area and surface displacement. *Bulletin of the Seismological Society of America* 84 (4): 974–1002.

Wijayanti E., F. Kristiawan, E. Purwanto, and S. Sangadji. 2016. Seismic vulnerability of reinforced concrete building based on the development of fragility curve: A case study. *Applied Mechanics and Materials* 845: 252–258. doi:10.4028/www.scientific.net/AMM.845.252

Yamaguchi, N., and F. Yamazaki. 2000. Fragility curves for buildings in Japan based on damage surveys after the 1995 Kobe earthquake. In Proceedings of the 12th conference on earthquake engineering, Auckland, New Zealand.

Chapter 3
Moment-Resisting Frames (MRFs)

3.1 Structural Model

In this section, six sets of model moment-resisting frames (MRF) were analyzed with different types of geometry (regular and irregular frames), material, and heights. These frames abide by the Eurocodes (EC). Each frame had three bays measuring 6 m each and identical height of 3 m for 3-, 6-, and 9-storey regular and irregular frames. The materials used are concrete and steel. Figure 3.1 shows the flowchart of the analysis, while Figs. 3.2 and 3.3 show the illustrated model for all storey heights.

The structures will use soil class A with peak ground acceleration (PGA), a_{gr}, which was assumed to be 0.5 g or 5 m/s^2. Based on EC8 (BSI 2004), type soil A is rock or other rock-like geological formations with at least 5 m of weaker material at the surface. Thus, to avoid the soil–structure interaction in the analysis, soil class A will be used. The importance value used was 1 and the behavior factor, *q,* was 4 for regular moment-resisting frame with medium ductility class (DCM). However, EC8 states that the behavior factor for irregular buildings decreases to 80% of the corresponding regular building.

The designs for MRCF were based on the existing building by using EC2 (BSI 2004) and EC8 (BSI 2004) standards. Several assumptions were made during the design of MRCF. Compressive stress of concrete was 30 N/mm^2 and yield stress of reinforcing steel was 460 N/mm^2. Tables 3.1 and 3.2 show the size of beam and column for regular MRCF and irregular MRCF, respectively.

3.2 Design Loads

All frames were imposed by the dead, live, and lateral loads. The lateral loads were designed based on EC8. The self-weight of the structures, weight of the permanent partition such as finishes, brick wall, and all permanent constructions are under dead load effect. The details of dead and live loads are as follows:

F. M. Nazri, *Seismic Fragility Assessment for Buildings due to Earthquake Excitation*, SpringerBriefs in Computational Mechanics,
https://doi.org/10.1007/978-981-10-7125-6_3

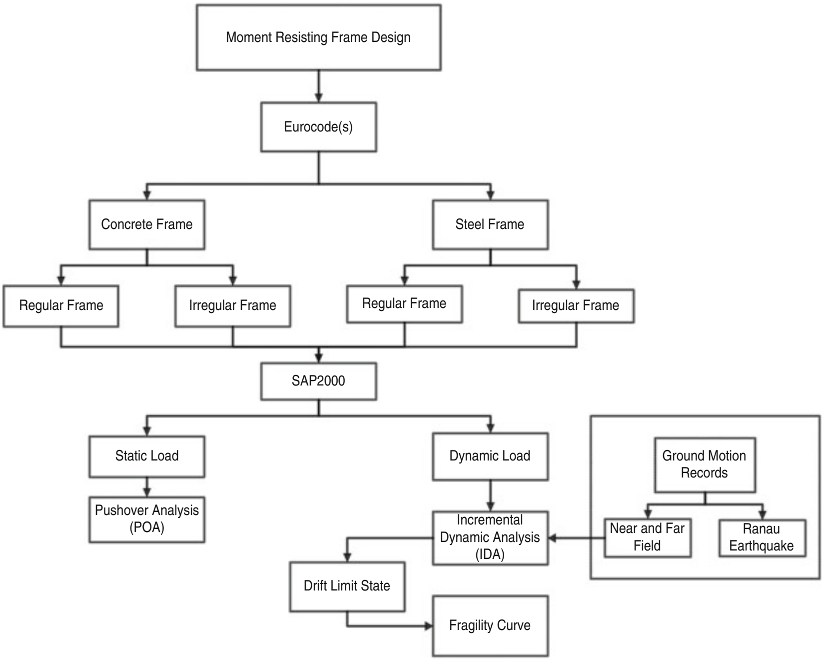

Fig. 3.1 General flow of chart methodology

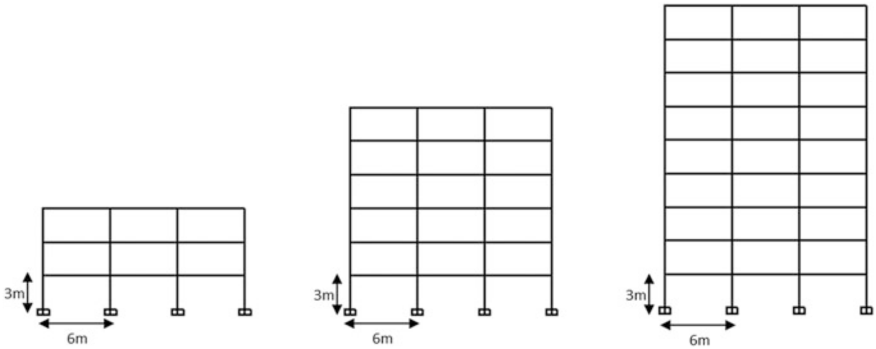

Fig. 3.2 Regular MRF

By assuming concrete density	= 24 kN/m^3,
The area of slab	= 36 m^2 (6 m × 6 m)
Thus, the self-weight of the slab	= concrete density × slab thickness (0.15 m)
	= 3.6 kN/m^2.

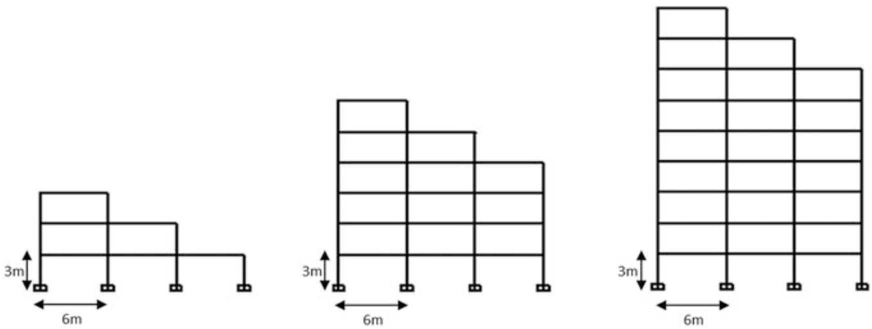

Fig. 3.3 Irregular MRF

Table 3.1 Size of beam and column for regular MRCF

Number of storey	3-Storey		6-Storey		9-Storey	
Section	Beam	Column	Beam	Column	Beam	Column
Size (mm)	350 × 500	500 × 500	350 × 500	500 × 500	350 × 500	500 × 500
Reinforcement	5T16	5T32	5T16	5T32	5T16	6T32
Shear link	8 mm @ 150 c/c		8 mm @ 150 c/c		8 mm @ 150 c/c	

Table 3.2 Size of beam and column for irregular MRCF

Number of storey	3-Storey		6-Storey		9-Storey	
Section	Beam	Column	Beam	Column	Beam	Column
Size (mm)	350 × 500	400 × 400	350 × 500	400 × 400	350 × 500	400 × 400
Reinforcement	4T16	3T20	5T16	4T20	5T16	4T20
Shear link	8 mm @ 150 c/c		8 mm @ 150 c/c		8 mm @ 150 c/c	

Tables 3.3 and 3.4 show the loads considered as the dead load and the live load, respectively.

The presence of masses associated with all gravity loads must be considered in the combination of actions. Therefore, from EC8 under Clause 3.2.4, the combination of seismic action is

$$W_{GQ} = \Sigma G_{k,j}{}'' + {}'' \Sigma \psi_{E,i} \cdot Q_{k,i}, \tag{3.1}$$

Table 3.3 Dead loads (G_k)

Dead load (G_k)	kN/m^2
Finishes	1.2
Self-weight slab	3.6
Services	0.5
Total	5.3

Table 3.4 Live loads (Q_k)

Live load (Q_k)	kN/m^2
Imposed load	1.5
Total	1.5

Table 3.5 Parameters recommended for type 1 elastic response spectra according to EC8

Ground type	S	T_b (s)	T_c (s)	T_d (s)
A	1.0	0.15	0.4	2.0

where

$$\psi_{Ei} = \varphi \cdot \psi_{2i} \tag{3.2}$$

For category A, storeys with correlated occupancies

$$\varphi = 0.8$$

For category A, domestic and residential areas

$$\psi_{2i} = 0.3$$

Thus, moment can be obtained by using Eq. (3.3):

$$M_{GQ} = \frac{W_{GQ} \cdot L}{12}, \tag{3.3}$$

where L is the length of bay in meter (m).

For horizontal components of seismic action, the design spectrum $S_d(T)$, base shear force, and horizontal forces were evaluated based on EC8.

Table 3.5 summarizes the parameters used in the development of elastic response spectrum for ground type A. Type 1 elastic response spectra were chosen since surface wave magnitude, M_s, is greater than 5.5.

3.3 Ground Motion Records

To perform IDA, one of the most important parameters in the analysis is the selection of ground motions. Thus, from the previous studies, three sets of ground motions were used in this research. The ground motions were chosen from the Pacific Earthquake Engineering Research Centre (PEER).

There are two types of ground motions considered in this study which are near-field (NF) and far-field (FF) ground motion. The criteria used to categorie NF

Table 3.6 Summary parameters of selected ground motion records for NF and FF

Type of Ground Motion	NF	FF
J–B distance	Less than 20 km	More than 20 km
Magnitude	5–7	5–7
Location	Any location	Any location

Table 3.7 Selective ground motion records for NF

Earthquake	Record name	Year	Station	Magnitude (M_w)	R_{jb} (km)
Imperial valley	RSN18	1953	El-Centro Array #9	5.50	15.11
San Fernando	RSN71	1971	Lake Hughes	6.61	17.22
Coyote lake	RSN146	1979	Gilray Array #1	6.74	10.21

Table 3.8 Selective ground motion records for FF

Earthquake	Name record	Year	Station	Magnitude (M_w)	R_{jb} (km)
Northwest Calif	RSN7	1941	Ferndale City Hall	6.60	91.15
Park Field	RSN32	1966	San Luis Obispo	6.19	63.34
Santa Barbara	RSN135	1978	Cachuma Dam Toe	5.92	23.75

and FF are based on Joyner–Boore distance (R_{jb}). The NF is less than 20 km, whereas the FF is more than 20 km (Li et al. 2015). The magnitude of ground motion records chosen was more than 5 since most of the earthquakes felt in Malaysia were having magnitude more than 5–7 which was categorized as moderate region earthquake. The summary of parameters of the selected ground motion records as tabulated in 13 (Table 3.6).

Based on the criteria aforementioned, three sets of ground motion records for the NF and FF were used as tabulated in Tables 3.7 and 3.8, respectively.

3.4 Development of Elastic Response Spectrum

Based on EC8, the elastic response spectrum can be developed. The value of parameters used is mentioned in Table 3.5. The elastic response spectra were developed from 0.4 to 2.0 g with an increment of every 0.4 g. Figure 3.4 shows the elastic response spectra for ground type A. The elastic response spectrum is used to scale-up or scale-down the ground motions.

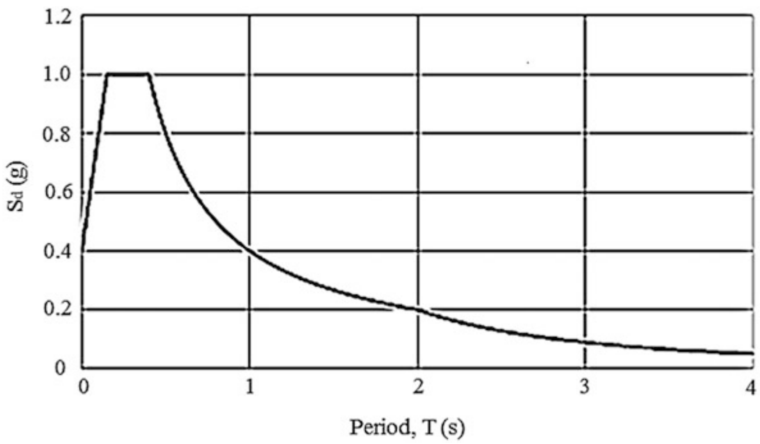

Fig. 3.4 Example type 1 elastic response spectra for ground type A (5% damping) (BSI 2004)

3.5 Scaling for Ground Motion Records

Before the scaling, the ground motion records from PEER NGA database were converted to the acceleration response spectrum (g) by using seismosignal software (Seismosoft 2011). After that, the acceleration time-history data were scaled according to the developed elastic response spectrum in order to match the characteristics of the ground motion to the soil type. The scaling was dependent on the value of frame fundamental period, T_1. Then, the scale factor will be used in SAP2000 to run IDA.

3.6 Fragility Curve

Five performance levels were studied which are operational phase (OP), immediate occupancy (IO), damage control (DC), life safety (LS), and collapse prevention (CP). Every limit state has their maximum drift limit. Xue et al. (2008) suggested the maximum drift limit and tabulated in Table 3.9.

Table 3.9 Maximum drift limit (%) (Xue et al. 2008)

Limit state	Drift (%)
OP	0.5
IO	1.0
DC	1.5
LS	2.0
CP	2.5

Then, mean and standard deviation for every limit state were calculated. For this study, Eq. (3.4) was used as it has already been simplified by Ibrahim and El-Shami (2011):

$$P[D/\mathrm{PGA}] = \Phi\left(\frac{\ln(\mathrm{PGA}) - \mu}{\sigma}\right), \tag{3.4}$$

where

D	damage
PGA	peak ground acceleration
Φ	standard normal cumulative distribution
M	mean
Σ	standard deviation of the natural logarithm of PGA .

Figure 3.5 shows the general steps to develop fragility curve.

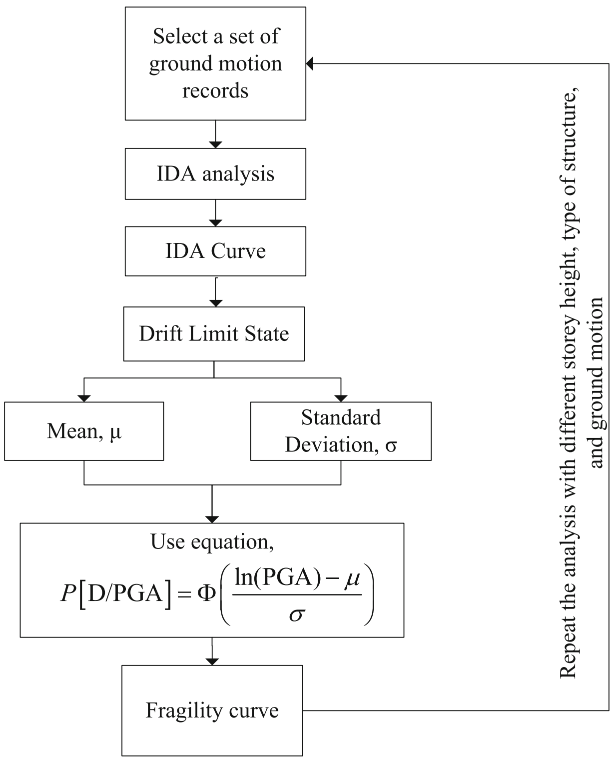

Fig. 3.5 General flow to develop fragility curve

References

BSI. 2004. *Eurocode 8: Design Provisions for Earthquake Resistance of Structures: Part 1-1, General Rules—Seismic Actions and General Requirements for Structures*. London: British Standards Institution.

Ibrahim, Y.E., and M.M. El-Shami. 2011. Seismic Fragility Curves for Mid-Rise Reinforced Concrete Frames in Kingdom of Saudi Arabia. *The IES Journal Part A: Civil & Structural Engineering* 4: 213–223. https://doi.org/10.1080/19373260.2011.609325.

Li, Y., F. Fan, and H. Hong. 2015. Influence of number of records and scaling on the statistics of seismic demand for lattice structure. *Thin-Walled Structures* 87: 115–126.

Seismosoft. 2011. Earthquake Engineering Software and Solutions. Retrieved December 2013, from http://www.seismosoft.com/en/SeismoSignal.aspx.

Xue, Q., C.-W.Wu, C.-C. Chen, and K.-C. Chen. 2008. The Draft Code for Performance-Based Seismic Design of Buildings in Taiwan. *Engineering Structures* 30, no. 6: 1535–1547.

Chapter 4
Performance of MRFs Due to Nonlinear Analysis

4.1 Performance of Regular and Irregular MRF Due to POA

4.1.1 Capacity Curves

Pushover analysis (POA) was carried out on six different types of frames. In this analysis, lateral load acts as the main role in evaluating the structure performance according to the pushover analysis. In this analysis, as suggested by Eurocode 8 (BSI 2004), the triangle lateral load was applied to perform the analysis.

POA was performed by incrementally increasing the magnitude of lateral load and analyzed using SAP2000 software (CSI 2004). Based on the results of this analysis, the capacity curve managed to be developed.

The percentage of drift was calculated using Eq. (4.1). In this study, the percentage of drift is limited to 3% because the maximum drift limit for the structure to collapse is 2.5% as suggested by Xue et al. (2008).

$$\text{Drift}(\%) = \frac{\Delta_{\text{max storey}}}{\sum_{\text{height of storey}}} \quad (4.1)$$

where,

Δ displacement of maximum storey

From the capacity curve, the drift performance will then be compared with the specific limit state mentioned earlier in Table 3.9. Figure 4.1 shows the capacity curves for moment resisting concrete frame (MRCF) for 3-storey, 6-storey, and 9-storey. According to the graph, maximum base shear for regular frame 3-storey is 413 kN at the drift of 1.60% while the maximum base shear for irregular frame is 277 kN at the drift of 1.00%. Maximum base shear for 6-storey regular frame is 370 kN at the drift of 1.30% while for the irregular frame is 301 kN at the drift of

F. M. Nazri, *Seismic Fragility Assessment for Buildings due to Earthquake Excitation*, SpringerBriefs in Computational Mechanics,
https://doi.org/10.1007/978-981-10-7125-6_4

Fig. 4.1 Capacity curve for MRCF of **a** 3-storey, **b** 6-storey, and **c** 9-storey

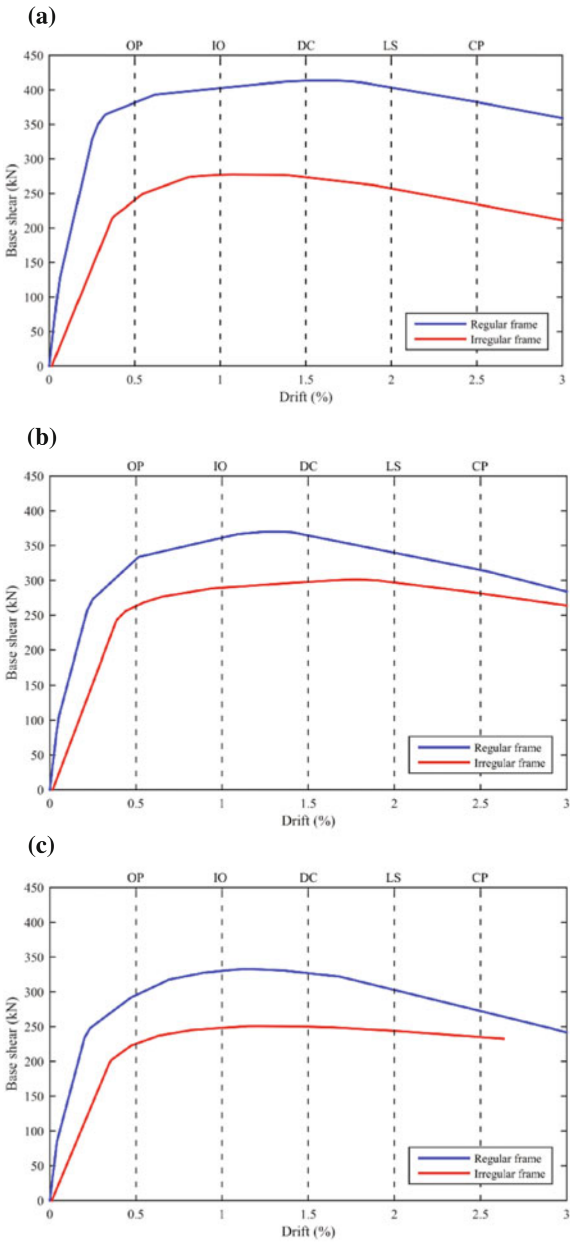

1.80%. Furthermore, the base shear of 9-storey regular frame is 333 kN at the drift of 1.10% which is greater than the base shear of 251 kN at the drift of 1.20%. From the result, it can be seen that the base shear of 3-storey is the highest compared to the 6-storey and 9-storey. This proves that low-rise frames have higher post-yield stiffness compared to the mid-rise and high-rise frames as stated by Nazri et al. (2015). In addition, most of the maximum base shear of MRCF regular and irregular frames occur from IO to DC state.

As compared to the irregular frames, the base shear of the regular 3-storey frame is 33% greater than the irregular whereas the base shear of the regular 6-storey frame is 19% greater than the irregular. Next, for the 9-storey frame structure, the base shear for regular is 25% greater compared to the irregular frame. In general, it can be concluded that regular frame shows the highest base shear for the 3-storey, 6-storey, and 9-storey frames. This shows the stiffness of structure and the irregularity frame affect the value of base shear.

As shown in Fig. 4.2, for the case of moment resisting steel frame (MRSF) , the maximum base shear for 3-storey, 6-storey, and 9-storey regular and irregular frames successfully achieved the collapse prevention state or CP with the limit drift of 2.5%. For the 3-storey regular and irregular base shear at the CP level are 320 and 190 kN, respectively. For 6-storey, the base shear of CP level for regular is 230 kN and the irregular is 170 kN. The base shear at CP stage for 9-storey regular is 300 kN while for the irregular is 170 kN. The results for MRSF indicate that the low-rise structure has the highest base shear compared to the mid-rise and high-rise.

When compared to the regular and irregular capacity curve, it can be seen that the regular frame has higher base shear compared to the irregular frame. For the case of regular 3-storey frame, the base shear increases to 41% compared to the irregular frame while for the 6-storey regular, it increases to 26%. Next, for the 9-storey frame, the base shear is 43% greater than the irregular frame. The pattern of the result was found similar to the MRCF result. The result shows that the irregularity influences the value of base shear, whereas the low-rise provides a higher base shear value.

4.1.2 Plastic Hinges

Apart from the capacity curve, plastic hinges can also be evaluated from the POA because it is one of the crucial properties in the analysis. The plastic hinges are based on the default hinge model which is defined in SAP2000. For beam section, the moment M3 hinge type was used as well as the column section, which is the Interacting P-M3. From the plastic hinges properties, the performance level for the structure can be known through color coding. The color coding will then be used to represent the performance level. Table 4.1 shows the type of color coding and its performance level. The status damage of the structure can be identified by observing the coloring code.

The performance level based on hinges properties of MRCF for regular and irregular frames with various heights are presented in Figs. 4.3, 4.4, and 4.5. As can be seen from the figures, most of the damage occurs at the beam section. However, not all frames are in the damage state because some are only in the collapse state.

Fig. 4.2 Capacity curve for MRSF **a** 3-storey, **b** 6-storey, and **c** 9-storey

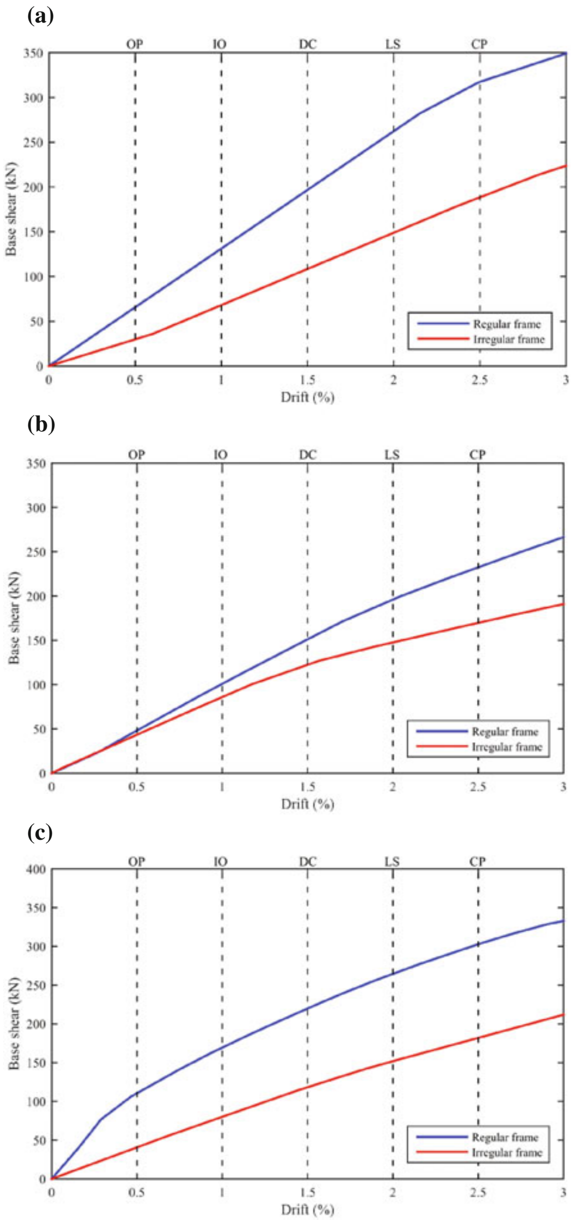

In addition, the deformations for all the regular frames happen at the bottom storey, while the deformation for the irregular frame starts at the top of the storey. This shows that the top storey for irregular frame is less stable and less stiff compared to the regular frame.

Table 4.1 Type of color coding with the plastic hinges

Type of color coding	Performance level	Definition
Red	E	Fail
Orange	D	Damage
Green	C	Collapse
Cyan	CP	Collapse prevention
Blue	LS	Life safety
Purple	IO	Intermediate occupancy
Pink	B	Yield

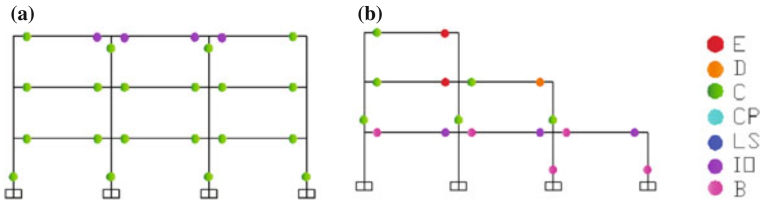

Fig. 4.3 Plastic hinges for MRCF 3-storey **a** regular and **b** irregular

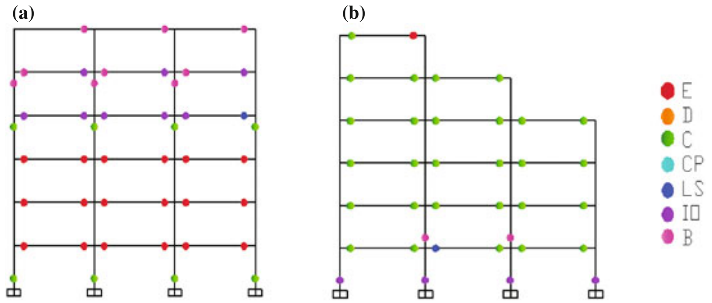

Fig. 4.4 Plastic hinges for MRCF 6-storey **a** regular and **b** irregular

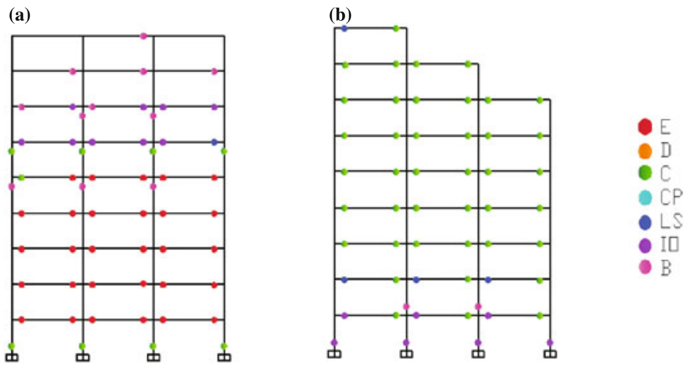

Fig. 4.5 Plastic hinges for MRCF 9-storey **a** regular and **b** irregular

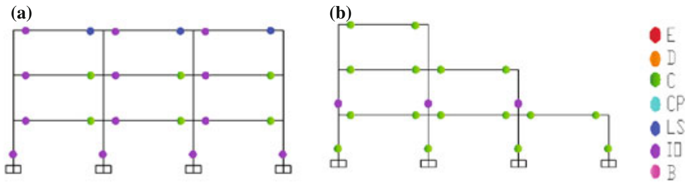

Fig. 4.6 Plastic hinges for MRSF 3-storey **a** regular and **b** irregular

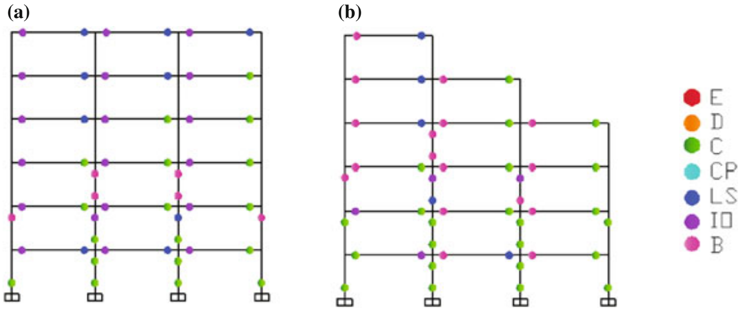

Fig. 4.7 Plastic hinges for MRSF 6-storey **a** regular and **b** irregular

However, the regular frame is more critical than the irregular frame because the deformation that occurs at the bottom storey has a higher potential to collapse all the structure.

Figures 4.6, 4.7, and 4.8 represent hinges properties of the regular and irregular MRSF for low-rise, mid-rise, and high-rise. According to the figure, all the frames only managed to achieve the collapse state. Similar to MRCF, the figure shows that most of the collapse states are formed at the beam sections, which cause failure start

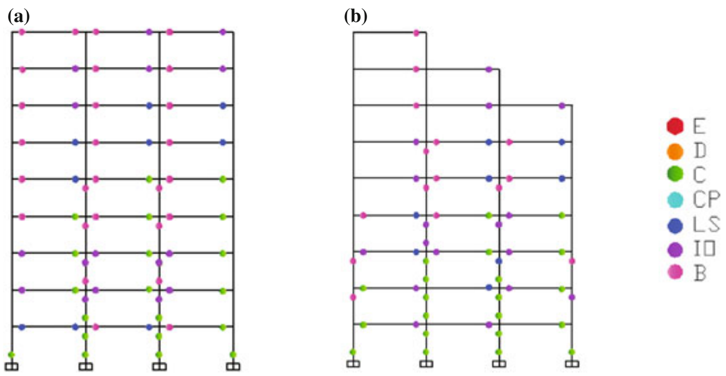

Fig. 4.8 Plastic hinges for MRSF 9-storey **a** regular and **b** irregular

at the beam section before the column section. In addition, the hinges distribution shows that the collapse state occur at the bottom storey for all frames except the regular 3-storey frame. This proves that the frames have low foundation stiffness and tend to collapse. However, the irregular for low-rise frame shows critical deformations because all the beam sections for every level are in the collapse state. In general, the regular frames for MRSF show a better performance compared to the irregular frame. It can also be clearly seen that the regular frame is stiffer than the irregular frame.

All the distributions of the hinges deformation are from maximum drift and base shear. The behavior of detailed MRCF and MRSF frames are adequate as indicated by the intersection of the demand capacity curves and the distribution of hinge in the beams and columns.

4.1.3 Interstorey Drift

The interstorey drift for MRCF and MRSF were plotted as illustrated in Figs. 4.9 and 4.10, respectively. The interstorey drift shows the drift for every storey and the comparison between the regular and irregular frames.

According to the graph in Fig. 4.9, it can be concluded that the regular frames are stiffer than the irregular frames. On top of that, the irregular frames provide a large percentage of drift. This proves that the irregular frames are unstable in design and only able to perform less compared to the regular frame.

Furthermore, the maximum storey drift occurs at the top of the storey for all frames. The maximum drift that occurs at the top of the 3-storey concrete frame for regular and irregular are 5 and 6%, respectively.

Meanwhile, the maximum drift for the 6-storey MRCF regular frame is 4% and the irregular frame is 11%, while for the 9-storey regular frame is 2.40% and the irregular frame is 7.40%. When comparing the drift percentage for the regular and irregular frames, the mid-rise and high-rise structures give a big difference in the drift percentage.

For MRSF shown in Fig. 4.10, the maximum drift that occurs at 3-storey are 4% for regular frame and 8% for the irregular frame. Meanwhile, the maximum drift for regular frame of 6-storey is 5% and irregular frame is 9%. The 9-storey MRSF for regular frame is 7.20% and irregular frame is 7.40%. For steel frame, a slight difference for regular and irregular frames only occur at 9-storey. According to the limit state, the drift for low-, mid-, and high-rise MRCF and MRSF exceeded the collapse prevention level.

Fig. 4.9 Interstorey drift for MRCF a 3-storey, b 6-storey, and c 9-storey

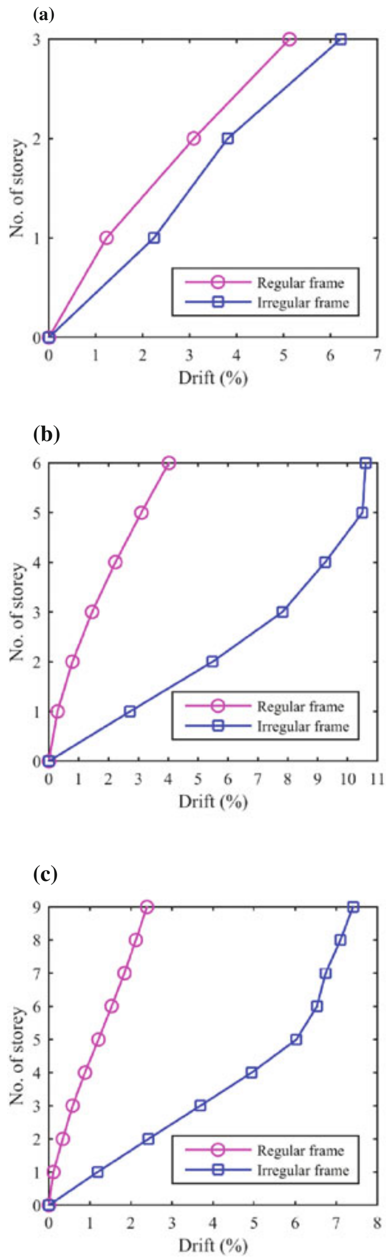

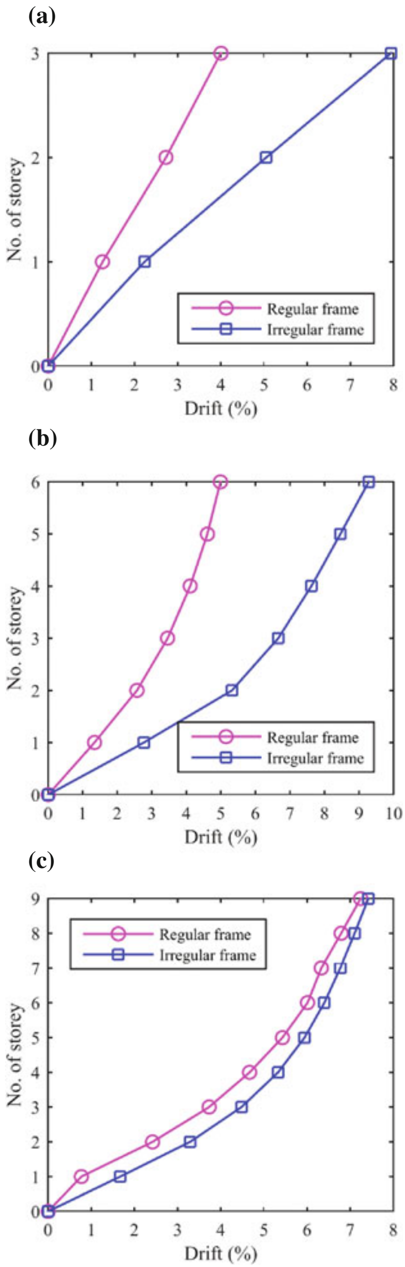

Fig. 4.10 Interstorey drift for MRSF **a** 3-storey, **b** 6-storey, and **c** 9-storey

4.2 Performance of Regular and Irregular MRFs Due to IDA

4.2.1 Near-Field (NF) Ground Motion Records

Figure 4.11 presents sample of the IDA curves obtained from the analysis of near-field (NF) records for MRCF regular and irregular frames structure under used ground motions, namely Imperial Valley, San Fernando, and Coyote Lake which labeled as RSN18, RSN71, and RSN146.

To evaluate the performance of structure, the mean drift was calculated from the IDA curve for every PGA and compared to the limit state as shown in Fig. 4.12. Based on the graph, the pattern is quite similar for the 3-, 6-, and 9-storey. The difference of PGA between the regular and irregular frame for 3-storey and 9-storey at DC state are 7 and 1%, respectively, which are considered as quite small. Meanwhile, for 6-storey, the difference of PGA at DC state is quite large which is 27%. This indicates that regular frame provides better performance compared to the irregular frame, which might be related to the selection of sizing and the ground

Fig. 4.11 IDA curves for MRCF based on NF

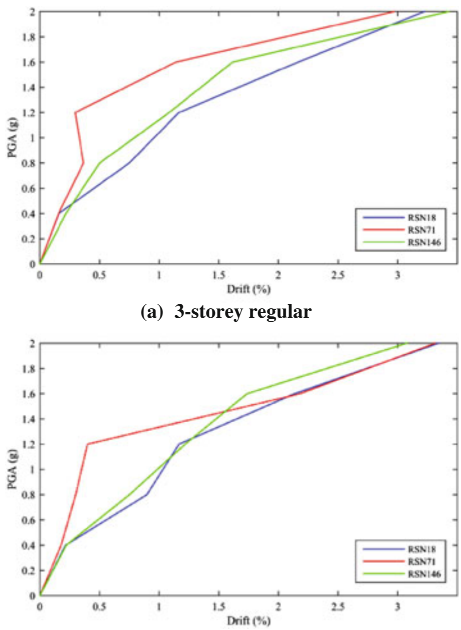

(a) 3-storey regular

(b) 3-storey irregular

Fig. 4.12 Mean IDA based on NF for MRCF

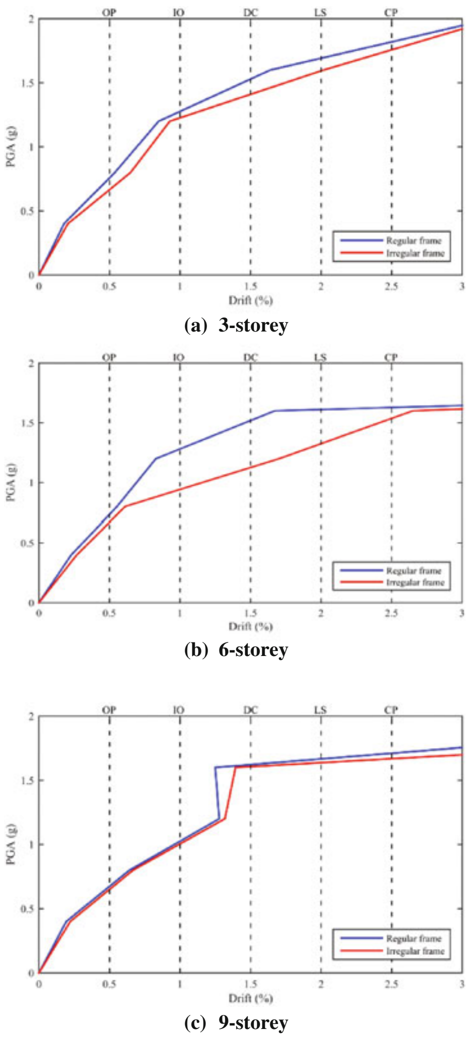

motion itself. For instance, a regular frame for 3-storey needs 1.50 g to achieve the DC limit state while only 1.40 g is needed for the irregular 3-storey frame.

Figure 4.13 shows sample of the IDA curves for regular and irregular MRSF under NF ground motion records.

The average IDA graph was plotted as shown in Fig. 4.14. From the graph, regular MRSF shows better performance compared to the irregular frame. As clearly shown, the drift difference at PGA 0.8 g of 3-storey MRSF between the regular and irregular frame shows a larger difference which is 38%. Generally, the pattern of IDA curve is different for each ground motion; hence, the pattern for IDA

Fig. 4.13 IDA curves for MRSF based on NF

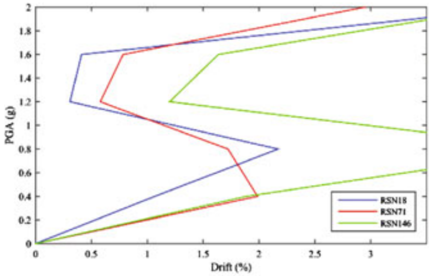

(a) 3-storey regular

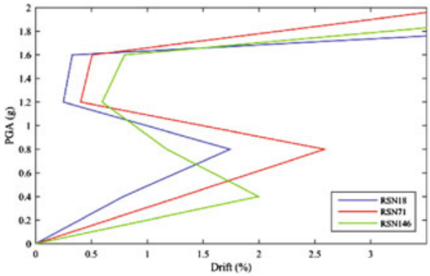

(b) 3-storey irregular

3-storey curve is a bit wavy compared to the 6-storey and 9-storey. This indicates that sometimes the lower damage measure values may be obtained for an increasing value of intensity measure compared to the one previously obtained for a lower intensity measure as stated by Kirçil and Polat (2006).

4.2.2 Far-Field (FF) Ground Motion Records

The pattern of IDA curves under far-field ground motions for 3-storey of regular and irregular frame is shown in Fig. 4.15. Another three sets of ground motion were used, namely Northwest Calif, Park Field, and Santa Barbara which are denoted as RSN7, RSN32, and RSN135, respectively.

Similar to NF ground motions, the mean of drift for FF ground motions are calculated and illustrated in Fig. 4.16. For FF analysis, the result is similar to NF ground motions. Overall, the result for 3-, 6-, and 9-storey show that the regular frame MRCF performs better than the irregular frame. Based on the mean result, 6-storey shows a larger difference between the regular and irregular frame compared to the low-rise and high-rise. For example, the mid-rise regular frame was achieved at CP state with PGA 1.90 g and PGA 1.60 g for the irregular frame.

Fig. 4.14 Mean IDA based on NF for MRSF

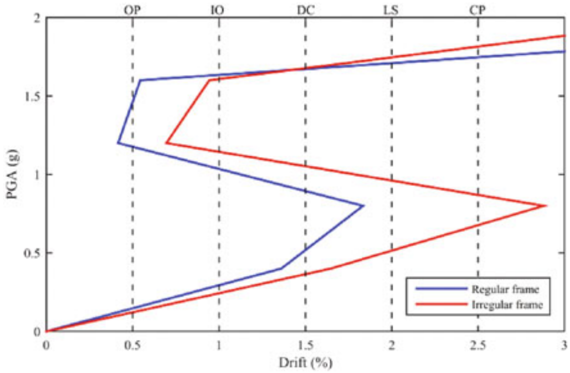

(a) **3-storey**

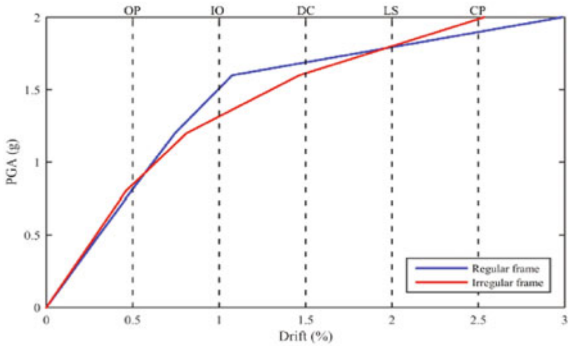

(b) **6-storey**

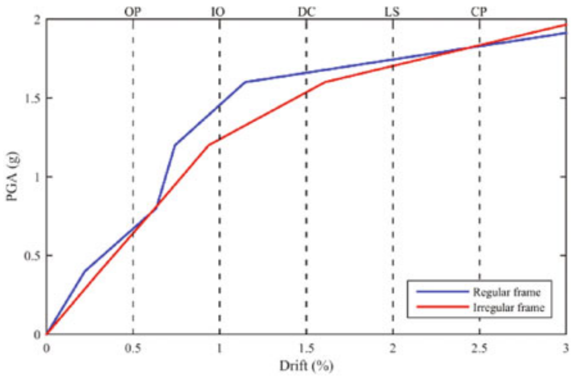

(c) **9-storey**

Fig. 4.15 IDA curves for MRCF based on FF

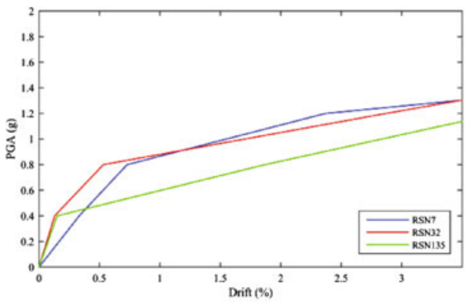

(a) 3-storey regular

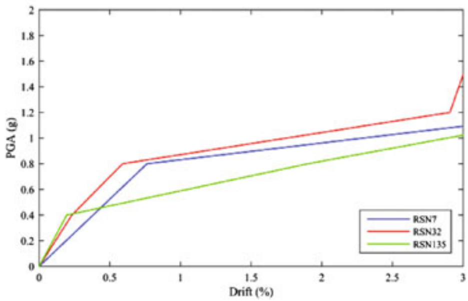

(b) 3-storey irregular

Figure 4.17 represents the graph for MRSF results under FF ground motions with different types of 3-storey height. It displays a wide range of behavior with large variation from a record to another record.

Following it, the mean IDA was calculated and the graph was plotted as shown in Fig. 4.18. Based on the observation, the obtained results show that the regular frame performs better. Among the low-, med-, and high-rise frame, the low-rise is unstable and might collapse first before other levels of storey. For example, a 3-storey regular frame needs 1.60 g while the irregular needs 1.40 g to reach the DC limit state. 1.60 g is needed for the regular and irregular 6-storey frames, whereas 1.70 g is needed for the regular 9-storey frame and 1.60 g for the irregular 9-storey.

4.3 Fragility Curve

The PGA was selected because it was used in the Incremental Dynamic Analysis (IDA). Next, Eq. (3.4) was applied to develop fragility curve. In this equation, two main parameters which are mean and standard deviation of PGA were calculated for every point which crosses the limit state vertical gridlines at the drift of 0.5, 1.0, 1.5, 2.0, and 2.5%. All the calculated parameters are tabulated in Tables 4.2, 4.3, 4.4, and 4.5.

Fig. 4.16 Mean IDA based on FF for MRCF

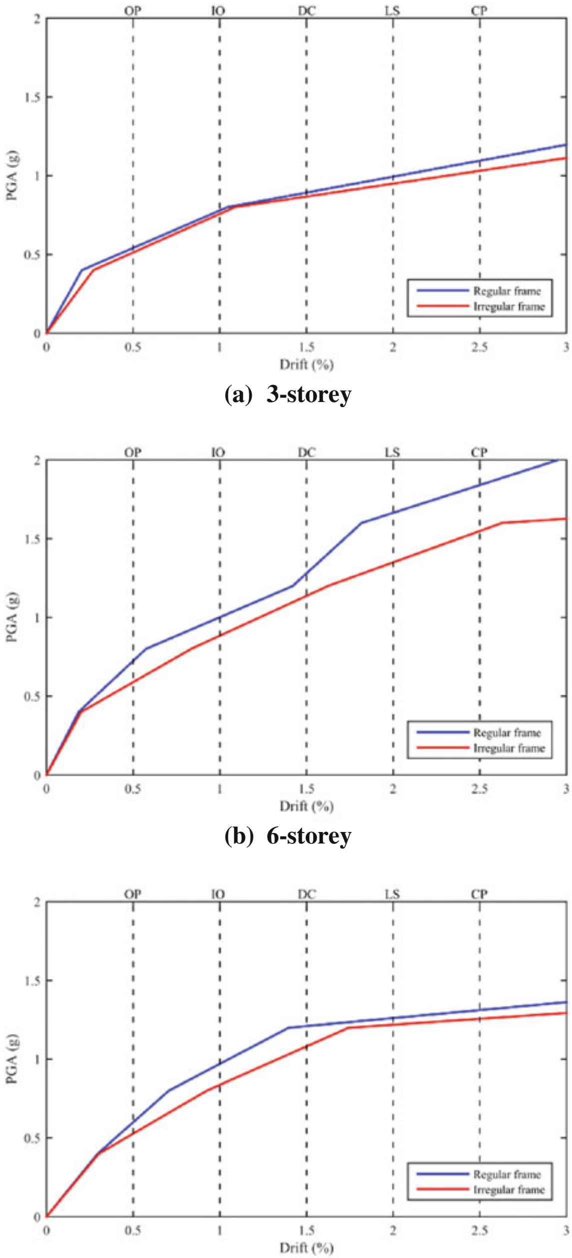

(a) 3-storey

(b) 6-storey

(c) 9-storey

Fig. 4.17 IDA curves for MRSF based on FF

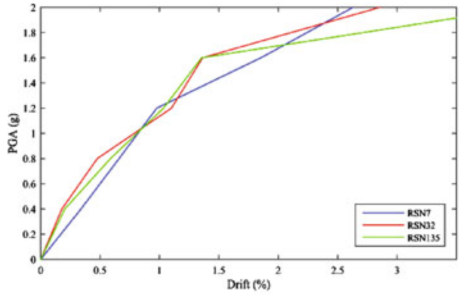

(a) 3-storey regular

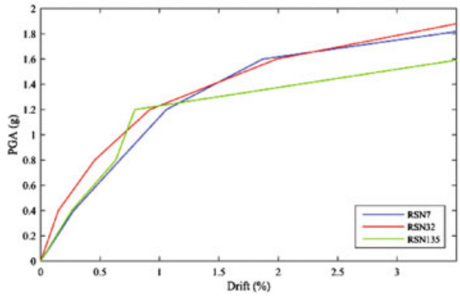

(b) 3-storey irregular

In this study, the seismic fragility is presented in the damage probability curve (fragility curve). All set of fragility curves were plotted. For instance, Fig. 4.19 shows the fragility curve for low-rise regular MRCF based on the near-field ground motions.

According to the figure illustrated, the performance of structure can be determined in terms of probability. For example, the probability of OP level is 0% when the PGA is 0.2 g which is considered as weak ground motions, but the probability of OP level is 98% when exposed to strong ground motion at PGA 1.8 g. In CP level, it starts to occur at PGA 1.6 g. The probability of CP level is 100% when the PGA is more than 2 g. Hence, this fragility curve can provide some ideas about the condition of the structure, in which the PGA starts from 0.2 g until 2.0 g based on the percentage of drift. In addition, the loss of damage can also be predicted using the fragility curve.

4.3.1 Fragility Curve for Near-Field (NF) Ground Motion Records

The fragility curves were compared according to different types of regularity. Figures 4.20, 4.21 and 4.22 show the fragility curve of MRCF for 3-storey, 6-storey, and 9-storey regular and irregular frame under NF.

Fig. 4.18 Mean IDA based on FF for MRCF

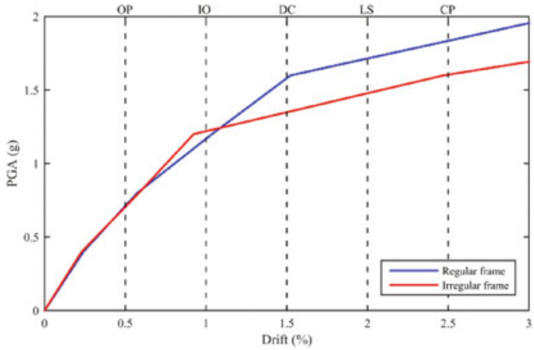

(a) 3-storey

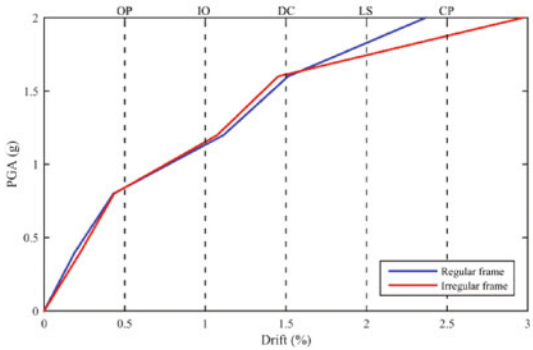

(b) 6-storey

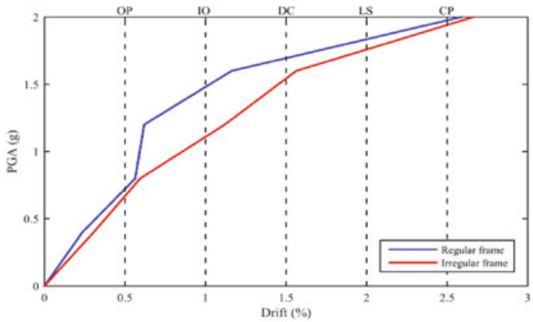

(c) 9-storey

The illustrated figures show the comparison between the regular and irregular frame. Based on Fig. 4.20, when the weak ground motions are exposed at 0.2 g, the probability of reaching or exceeding the regular low rise is 0% and the irregular frame is 0%. At the CP level, the probability for regular frame is 100% when the ground motion is more than 2.0 g and the irregular frame is 1.90 g.

For 6-storey, the probability of OP level is 100% for regular frame when the ground motion is 1.0 and 1.70 g for irregular frame. Meanwhile, for CP level, 100%

Table 4.2 Parameters of log-normal distribution for concrete frame based on near-field records

No. of storeys	OP		IO		DC		LS		CP	
	M	σ	μ	σ	μ	σ	μ	σ	μ	σ
Regular frame										
3	0.14	0.39	0.21	0.20	0.42	0.11	0.51	0.08	0.59	0.05
6	0.32	0.11	0.29	0.04	0.45	0.03	0.48	0.01	0.50	0.02
9	0.40	0.14	0.13	0.32	0.47	0.05	0.53	0.03	0.056	0.03
Irregular frame										
3	0.28	0.42	0.08	0.20	0.35	0.04	0.48	0.06	0.56	0.05
6	0.34	0.07	0.01	0.15	0.13	0.16	0.51	0.03	0.53	0.02
9	0.37	0.23	0.18	0.41	0.32	0.19	0.51	0.03	0.53	0.02

Table 4.3 Parameters of log-normal distribution for concrete based on far-field records

No. of storeys	OP		IO		DC		LS		CP	
	M	σ	μ	σ	μ	σ	μ	σ	μ	Σ
Regular frame										
3	0.26	0.35	0.07	0.43	0.06	0.39	0.16	0.36	0.24	0.33
6	0.30	0.13	0.01	0.03	0.24	0.09	0.52	0.03	0.63	0.05
9	0.42	0.23	0.02	0.19	0.20	0.05	0.26	0.04	0.31	0.05
Irregular frame										
3	0.53	0.15	0.12	0.40	0.01	0.38	0.09	0.35	0.23	0.30
6	0.45	0.22	0.15	0.16	0.12	0.08	0.34	0.06	0.45	0.03
9	0.61	0.15	0.15	0.13	0.14	0.06	0.22	0.03	0.28	0.06

Table 4.4 Parameters of log-normal distribution for steel frame based on near-field records

No. of storeys	OP		IO		DC		LS		CP	
	M	σ	μ	σ	μ	σ	μ	σ	μ	Σ
Regular frame										
3	1.11	1.32	0.44	0.94	0.17	0.71	0.12	0.61	0.23	0.59
6	0.23	0.05	0.47	0.15	0.51	0.10	0.56	0.09	0.61	0.09
9	0.40	0.41	0.27	0.21	0.42	0.13	0.50	0.10	0.63	0.05
Irregular frame										
3	0.65	1.23	0.26	0.84	0.05	0.53	0.10	0.66	0.24	0.47
6	0.14	0.13	0.33	0.13	0.48	0.10	0.58	0.08	0.64	0.04
9	0.04	0.42	0.36	0.28	0.39	0.23	0.52	0.12	0.59	0.06

Table 4.5 Parameters of log-normal distribution for steel frame based on far-field records

No. of storeys	OP		IO		DC		LS		CP	
	M	σ	μ	σ	μ	σ	μ	σ	μ	σ
Regular frame										
3	0.36	0.16	0.15	0.04	0.45	0.07	0.55	0.03	0.63	0.04
6	0.17	0.03	0.12	0.03	0.44	0.12	0.61	0.06	0.66	0.04
9	0.40	0.51	0.16	0.39	0.42	0.22	0.52	0.17	0.56	0.16
Irregular frame										
3	0.36	0.17	0.18	0.05	0.35	0.06	0.43	0.09	0.48	0.10
6	0.09	0.11	0.26	0.22	0.42	0.23	0.50	0.18	0.59	0.12
9	0.05	0.37	0.41	0.16	0.50	0.12	0.58	0.07	0.67	0.03

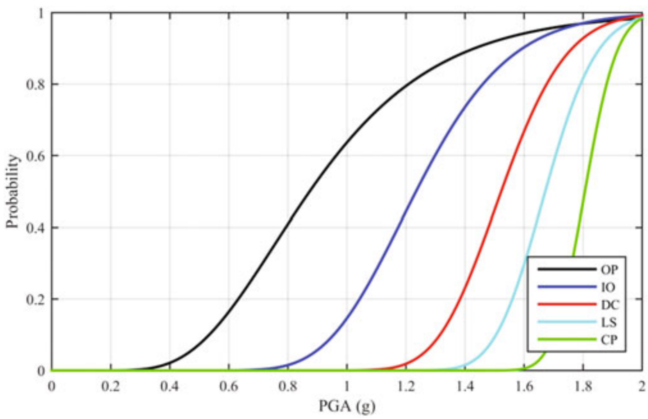

Fig. 4.19 Fragility curve for low-rise regular MRCF based on near-field ground motions

probability can be achieved when the ground motion is 1.70 g for the regular while for the irregular frame is 1.80 g. For 9-storey, when the PGA is 0.60 g, the 20% probability indicates that OP performance level can occur for regular frame and 24% for irregular frame. For regular frame, the ground motion which is more than 1.90 g will give 100% probability of reaching and exceeding the CP level and 1.80 g ground motion for the irregular.

Generally based on the graph, it can be concluded that irregular frames provide less performance compared to regular frames when the weak or strong ground motions are exposed to low-, mid-, and high-rise MRCF.

Figures 4.23, 4.24 and 4.25 present the fragility curve for 3-, 6-, and 9-storey for regular and irregular frame based on steel frame under NF.

According to Fig. 4.23, when the PGA is 0.4 g, the OP level for regular frame has the probability of approximately 55% while the irregular frame is 40%. At the CP level, the probability is 2% for regular and 0% for irregular frame. However, when the PGA is 1.8 g, the probability of reaching or exceeding the OP level for

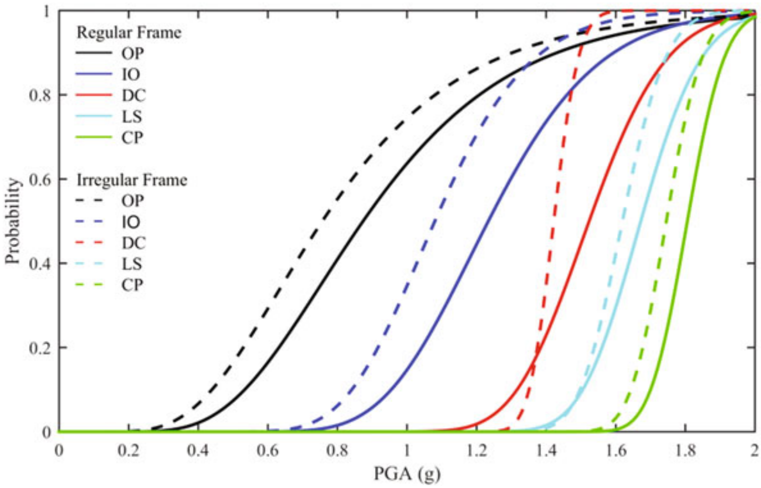

Fig. 4.20 Fragility curve for concrete 3-storey regular and irregular frames under NF

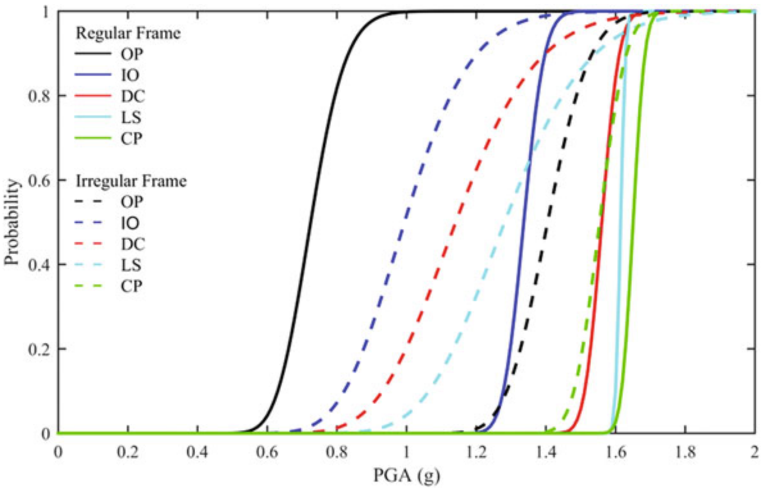

Fig. 4.21 Fragility curve for concrete 6-storey regular and irregular frames under NF

both the regular and irregular is approximately 90 and 84% respectively, whereas at the CP level, the probability for regular is 70% and irregular is 76%.

However for 6-storey MRSF, when PGA at 0.8 g was triggered, the probability of OP level for regular and irregular frame are 40 and 20% respectively, while the probability of CP level for both the regular and irregular frame is 0%. However, when the PGA is 2.0 g, the probability of reaching and exceeding the OP is 100% for both frames and CP level is approximately 84 and 90% for regular and irregular

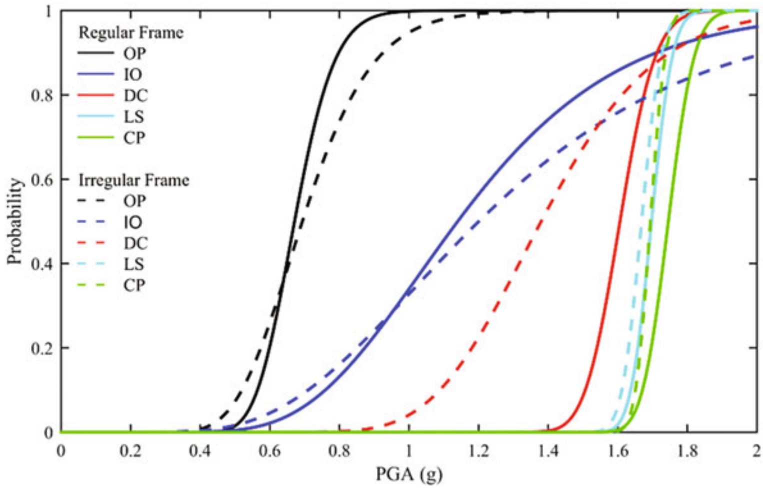

Fig. 4.22 Fragility curve for concrete 9-storey regular and irregular frames under NF

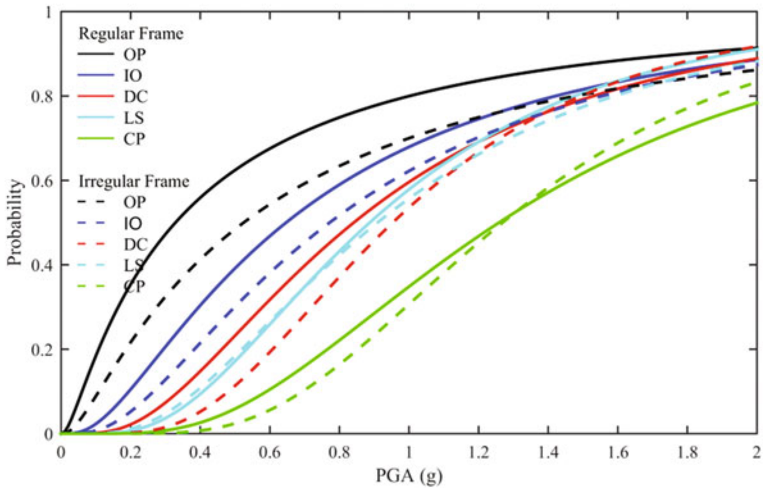

Fig. 4.23 Fragility curve for steel 3-storey regular and irregular frames under NF

frame. For 9-storey, the probability of CP level with 100% occur when the PGA is 2.1 g for both the regular and irregular frames.

According to the observations conducted, the pattern is different from the fragility curve based on the concrete material. For steel, the regular frame provides a higher percentage of probability curves at the OP and CP level.

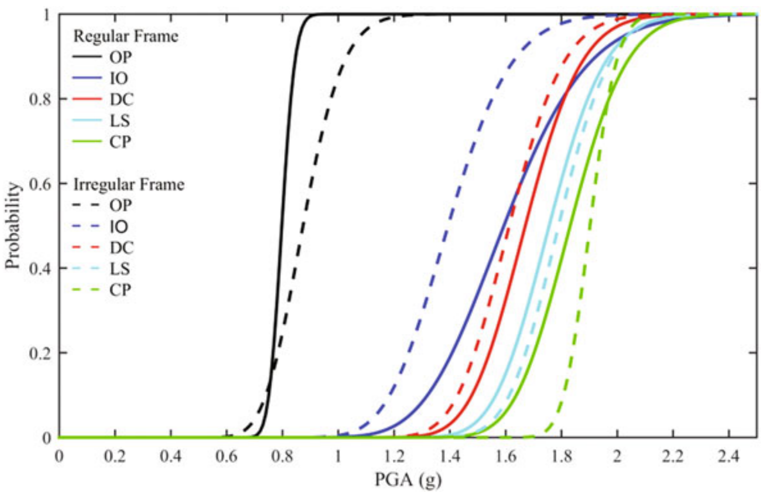

Fig. 4.24 Fragility curve for steel 6-storey regular and irregular frames under NF

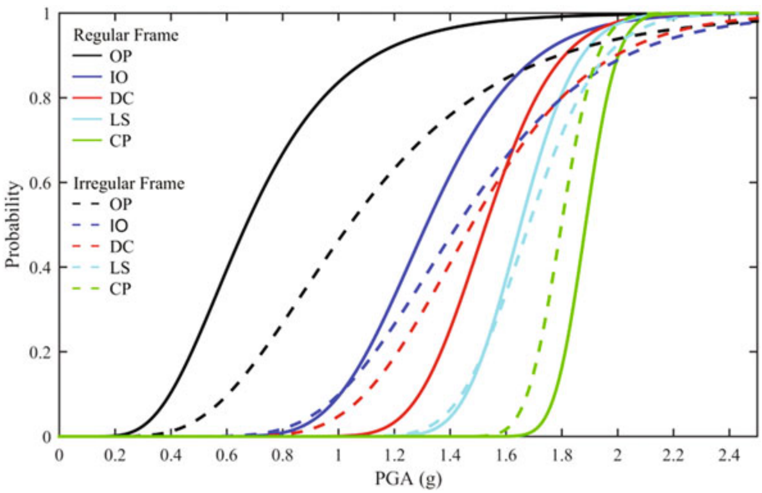

Fig. 4.25 Fragility curve for steel 9-storey regular and irregular frames under NF

4.3.2 Fragility Curve for Far-Field (FF) Ground Motion Records

Figures 4.26, 4.27, and 4.28 show the fragility curve for low-, mid-, and high-rise of both the MRCF regular and irregular frames under FF.

Based on Fig. 4.26, the probability of reaching or exceeding the OP state at 0.6 gfor MRCF irregular frame for low-rise is 52% and regular frame is 24%.

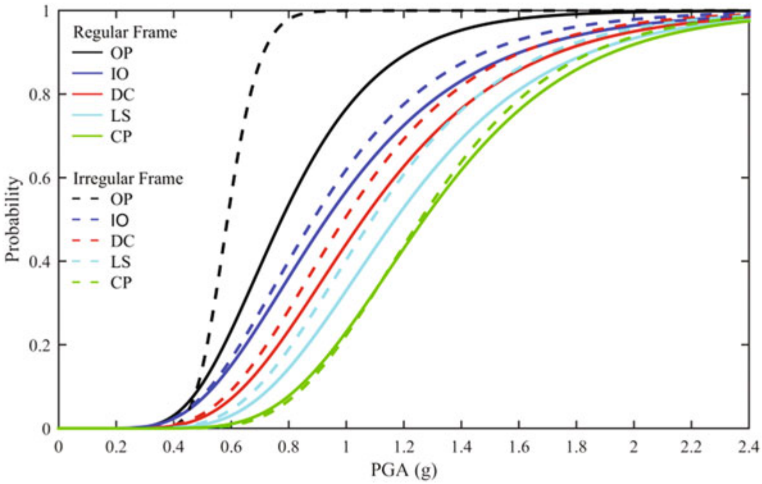

Fig. 4.26 Fragility curve for concrete 3-storey regular and irregular frames under FF

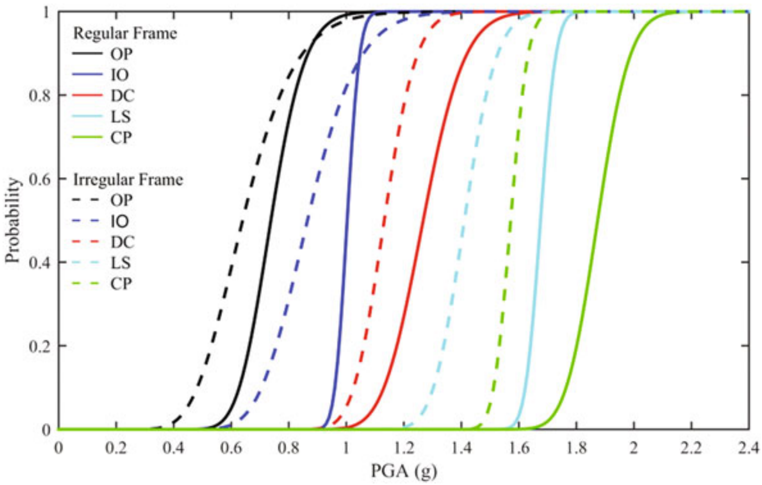

Fig. 4.27 Fragility curve for concrete 6-storey regular and irregular frames under FF

However, when the PGA is 1.8 g, the probability of OP is approximately 100% for both the regular and irregular frames. Meanwhile, the probability of reaching or exceeding the CP level is 2% for both frames when PGA is 0.6 g. Other than that, the probability of CP for irregular frame is 90% and regular frame is 88% when the PGA is 1.8 g.

For mid-rise frame with PGA 0.6 g, the probabilities of OP are 4 and 38% for regular and irregular frame, respectively. The probability of OP is 100% for both frames when PGA is more than 1.0 g. At the CP level, the probability is 100%

when the PGA is 1.7 g for irregular frame and PGA is 2.1 g for regular frame. The probability of OP for high-rise irregular MRCF is 72% and the regular frame is 38% when the PGA is 0.6 g. The probability of OP is 100% when PGA is 0.8 g for irregular frame. Aside from that, the probability of reaching or exceeding the CP state is 100% when the PGA is 1.6 g for both frames.

Figures 4.29, 4.30, and 4.31 present the fragility curve for 3-, 6-, and 9-storey MRSF for both the regular and irregular frames under FF round motions.

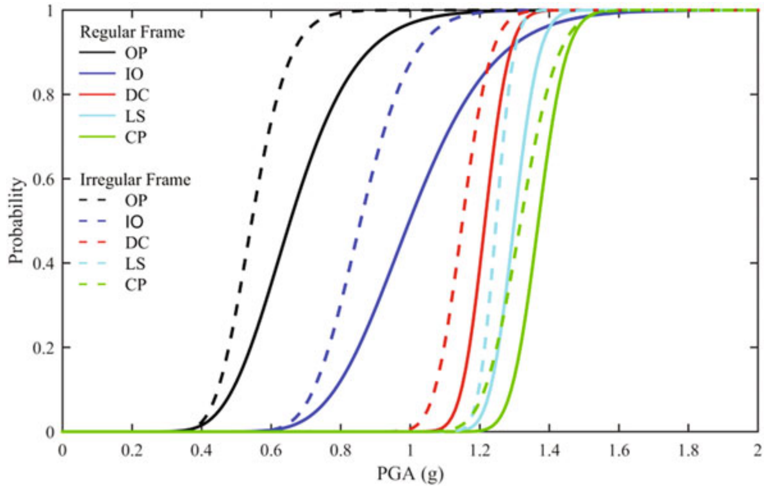

Fig. 4.28 Fragility curve for concrete 9-storey regular and irregular frames under FF

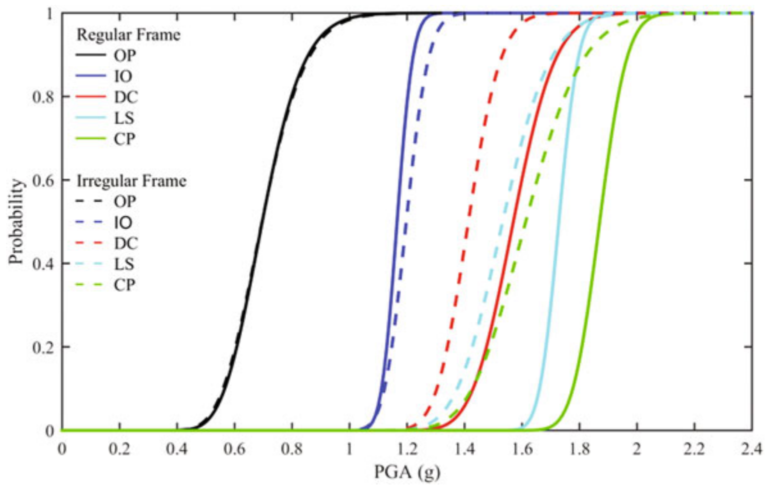

Fig. 4.29 Fragility curve for steel 3-storey regular and irregular frames under FF

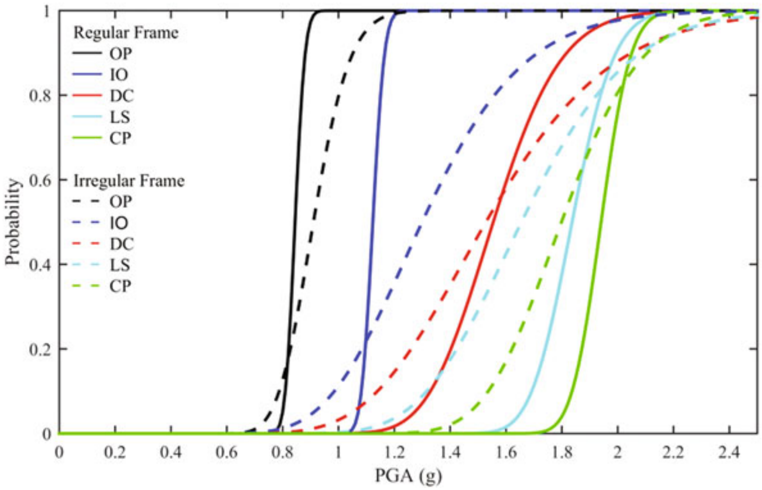

Fig. 4.30 Fragility curve for steel 6-storey regular and irregular frames under FF

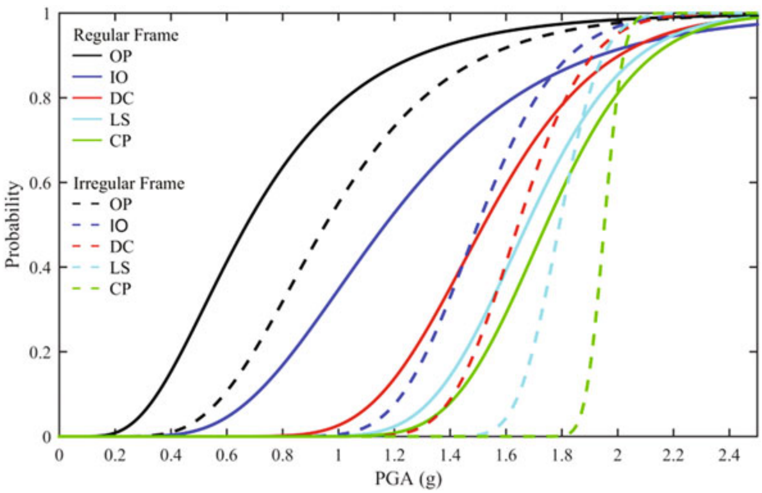

Fig. 4.31 Fragility curve for steel 9-storey regular and irregular frames under FF

Hence, when the ground motions are exposed to PGA 0.6 g, the probability of reaching or exceeding OP level is 20% for 3-storey regular and irregular MRSF, whereas for PGA 1.1 g, the probability for both frames are similar which is 100%. In addition, the probability of reaching and exceeding the CP level for 3-storey irregular and regular frame is 100% when the ground motion of PGA is more than 2.0 g.

For 6-storey with PGA 0.8 g, the probability of OP is 2% and 14% for regular and irregular frame, respectively, while the probability of OP level is 100% when the PGA is 0.9 g for regular and 1.2 g for irregular frame.

However, the probability of CP is 100% when the PGA is 2.2 and 2.4 g for regular and irregular frame, respectively. The probability of reaching or exceeding OP state is 40 and 10% for 9-storey regular and irregular frame with PGA of 0.6 g. Meanwhile, the probability of reaching or exceeding CP state is 100% when the PGA is 2.4 g for regular and 2.2 g for irregular frame.

For FF records, the irregular concrete frame has a higher probability of reaching and exceeding both the OP and CP level for weak and strong ground motions. In contrast, if the material is steel, the probability of reaching and exceeding the OP and CP level for regular frame is higher compared to the irregular frame.

References

BSI. 2004. *Eurocode 8: Design Provisions for Earthquake Resistance of Structures: Part 1-1, General Rules—Seismic Actions and General Requirements for Structures*. London: British Standards Institution.

CSI. 2004. *SAP2000 Integrated Finite Element Analysis and Design of Structures*, v10ed. Berkeley: Computer and Structures Inc. (CSI).

Kirçil, M.S., and Z. Polat. 2006. Fragility analysis of mid-rise R/C frame buildings. *Engineering Structures* 28 (9): 1335–1345.

Nazri, F.M., T.C. Ghuan, S.N. Hussin, and T.A. Majid. 2015. Evaluation of soil flexibility of the reclaimed area in Penang using the non-destructive method. *Natural Hazards*: 1–25.

Xue, Q., C.-W. Wu, C.-C. Chen, and K.-C. Chen. 2008. The draft code for performance-based seismic design of buildings in Taiwan. *Engineering Structures* 30(6): 1535–1547.

Chapter 5
Closing Remarks

The purpose of this book is to develop fragility curves for regular and irregular frames. Regular and irregular frames based on concrete (MRCF) and steel frames (MRSF) for low-, mid-, and high-rise were designed based on Eurocode 2, Eurocode 3, and Eurocode 8. The pushover analysis (POA) and incremental dynamic analysis (IDA) were performed by using the SAP2000 software. For the dynamic analysis, three sets of near-field (NF) ground motion and far-field (FF) ground motion were used. Besides, the performance of regular and irregular frames due to static and dynamic load was evaluated and included in this book. The following conclusions can be drawn:

i. Based on the POA for MRCF, the capacity curves for regular and irregular frames were compared. Regular frames show a higher base shear compared to irregular frames for all storeys. The base shear increased by 33, 19, and 25% for 3-, 6-,and 9-storey, respectively. While for the MRSF, it also shows the same pattern in which the base shear for regular frames is higher compared to irregular frames. The base shear increased by 41% for 3-storey, 26% for 6-storey, and 43% for 9-storey. It shows that regular frames have a higher demand than irregular frames for both concrete and steel frames.
ii. The IDA curve for regular frames was compared with irregular frames. Based on the observation of the IDA curve under NF ground motions, it shows that regular frames give a better performance compared to irregular frames for low-, mid-, and high-rise structures for both concrete and steel materials. For a regular 3-storey MRCF, it can sustain up to 1.70 g before collapsing compared to irregular frames that can only sustain 1.80 g. For 6-storey MRCF, regular frames need 1.50 g to achieve the DC state and irregular frames need 1.10 g. For 9-storey MRCF, regular frames need 1.70 g and irregular frames need 1.60 g to achieve the collapse state. Meanwhile, for frames made using steel material, the difference between the IDA curves for regular and irregular frames is not too significant. Meanwhile, for the analysis under the FF ground motions, regular frames show a better performance for both MRCF and MRSF.

F. M. Nazri, *Seismic Fragility Assessment for Buildings due to Earthquake Excitation*, SpringerBriefs in Computational Mechanics,
https://doi.org/10.1007/978-981-10-7125-6_5

iii. The fragility curves were developed for regular and irregular MRCF and MRSF based on specific structural performance level. Fragility curve is a unique curve at specific buildings which will have its own curve. As a comparison of fragility curves between regular and irregular frames based on the ground motion records at NF for low-rise MRCF, the highest probability of reaching and exceeding the performance levels was observed in irregular frames at lower PGA. However, for mid-rise MRCF it was a bit different, regular frames show a lower PGA as they achieved 100% of the OP and CP levels at PGA 1.0 and 1.70 g. For high-rise, irregular frames demonstrate less performance compared to regular frames. However, for all storeys of MRSF, it can be concluded that regular frames give a higher percentage of probability curve at the performance levels. Under FF ground motions, irregular MRCF frames for all types of storey give higher probability of reaching the performance levels. On the other hand, for MRSF, regular frames show higher probability of reaching or exceeding the performance levels.

Appendix A
Design of Regular and Irregular Moment-Resisting Concrete Frames (MRCF)

F. M. Nazri, *Seismic Fragility Assessment for Buildings due to Earthquake Excitation*, SpringerBriefs in Computational Mechanics,
https://doi.org/10.1007/978-981-10-7125-6

	UNIVERSITI SAINS MALAYSIA	
	School of Civil Engineering	
Project : Seismic Concrete Frame Design Based on Eurocode for 3-storey		

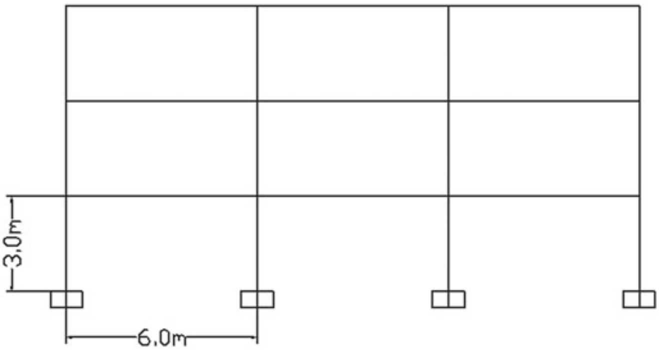

Floor height =	3	m
Bay width =	6	m
Area =	36	m^2

Project : Seismic Concrete Frame Based on Eurocode for 3-storey		
Ref. / Code	**Calculation**	**Output**
	1st Floor Slab Action Calculation:	
	Dead Load (Gk)	
	Dead Load (DL) — **kN/m²** Finishes — 1.2 S/w Slab* — 3.6 Services — 0.5 **TOTAL** — 5.3 x Area (m²)	
	*Concrete density x thickness (0.15m)	
	Hence, Total Gk = 190.8 kN	
	Live Load (Qk)	
	Live Load (LL) — **kN/m²** Imposed load — 1.5 **TOTAL** — 1.5 x Area (m²)	
	Hence, Total Qk = 54 kN	
EC 8 Cl 3.2.4	Combination of the seismic action with other load.	
Eq 3.17	$W_{GQ} = \Sigma G_k \text{ '+' } \Sigma \psi_{Ei} Q_k$	
	where,	
Eq 4.2	$\psi_{Ei} = \varphi . \psi_{2i}$	
Table 4.2	For category A, storeys with correlated occupancies; φ = 0.8	
EC 0 Table A1.1	For category A, domestic and residential areas; ψ_{2i} = 0.3	
	Thus, ψ_{Ei} = 0.24	
	Total factored load, W_{GQ} : 203.76 kN	**W_{GQ} = 203.76kN**

Project : Seismic Concrete Frame Based on Eurocode for 3-storey		
Ref. / Code	**Calculation**	**Output**
	Maximum bending moment (approx.) :	
	M_{GQ} = (WGQ . L) /12 ; L = 6m	
	M_{GQ} = 101.88 kNm	**M_{GQ} = 101.88kN**
	Horizontal Seismic Action:	
	Parameters:	
EC 8		
Eq 4.6	$T_1 = C_t.H^{3/4}$	
	where,	
	$C_{t\ (Concrete)}$ = 0.075	
Fig. 1(a)	H = 9 m	
	Hence,	
	T_1 = 0.39 s	
Table 3.2	For type 1 elastic response spectra;	
	Ground type : A	
	S : 1	
	Tb : 0.15s	
	Tc : 0.4s	
	Td : 2s	
	Thus,	
	T_1 in range of Tb and Tc (Tb ≤ T1 ≤ Tc)	
	Since Tb ≤ T1 ≤ Tc , use equation 3.15.	
Eq 3.15	Sd(T1) = ag . S . (2.5/q)	
Cl 3.2.1(3)	$a_g = a_{gR} . \gamma_I$	
	where,	
Cl 3.2.1(3)	γI : 1	
Cl 3.2.1(2)	agR : Peak ground acceleration on type A ground* (Assume 0.5g)	
	so, ag = 0.08 g = 0.78 m/s²	

Project : Seismic Concrete Frame Based on Eurocode for 3-storey		
Ref. / Code	**Calculation**	**Output**
Cl 6.3.2	Behaviour factor (q)	
Table 6.2	q : 4 ; For moment resisting frame (DCM)	
Eq 3.15	Sd(T1) = ag . S . (2.5/q)	
	Sd(T1) = 0.49 m/s²	
Cl 4.3.3.2.2	λ = 1	
	For the total mass of the building, *m*	
	m = (WGQ.nb.ns)/g	
	which,	
	nb : number of bays	
	ns : number of storeys	
	So,	
	m = 1833.84 kN	
	Base Shear Force :	
Cl 4.3.3.2.2	Base shear force, fb	
	Fb = Sd(T1) . *m* . λ	
	Fb = 893.997 kN	**Fb = 893.997 kN**

Project : Seismic Concrete Frame Based on Eurocode for 3-storey

Ref. / Code	Calculation	Output
	Horizontal sotrey seismic action calculatio:	
Cl 4.3.3.2.2	Distribution of the horizontal seismic force	
	Σzi.mi = (3 x 135.22) + (6 x 135.22) + (9 x 135.22)	
	Σzi.mi = 33009.12	
Cl 4.3.3.2.3(3) Eq 4.11	Fi = Fb . (zi.mi/Σzi.mi)	
	F3 = 447.00 kN	
	F1 = 298.00 kN	
	F2 = 149.00 kN	

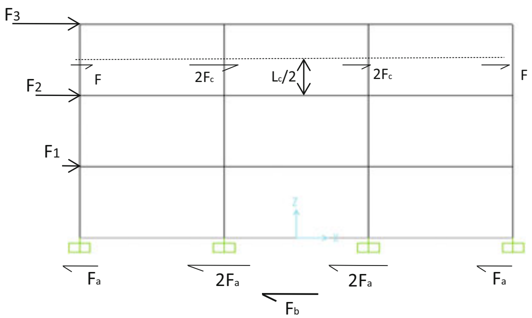

Ref. / Code	Calculation	Output
	Assume, the interrior column is twice as large as exterior column.	
	So,	
	6Fa = Fb	
	Fa = 149.00 kN	
	and	
	6Fc = 149.00 kN	
	Fc = 24.83 kN	

Project : Seismic Concrete Frame Based on Eurocode for 3-storey		
Ref. / Code	**Calculation**	**Output**
	Maximum bending moment from sway load : M_E = Fa.Lc + (Fc.Lc/2) ; Lc = 3.0 m M_E = 484.25 kNm Total moment, M_T $M_T = M_E + M_{GQ} \geq$ Mstatic Wstatic = $1.35G_k + 1.5Q_k$ Mstatic = (Wstatic . L) / 12 ; L = 6m Mstatic = 169.29 kNm	**Mstatic = 169.29kNm**
	Thus, M_T = 586.13 $\geq$ Mstatic $M_T \geq$ Mstatic	**OK**

Project : Seismic Concrete Frame Based on Eurocode for 3-storey		
Ref. / Code	**Calculation**	**Output**
	RC Beam Design :	
	Assume,	
	Bar diameter = 20 mm	
	Link diameter = 10 mm	
	Cover to reinforcement = 25 mm	
	Concrete strength = 30 N/mm²	
	Steel yield stress = 460 N/mm²	
	Beam width = 350 mm	
	Beam depth = 500 mm	
	d = 700 - 25 - 20/2 -10	
	d = 455 mm	
EC2 Cl 6.1	K = $\frac{M}{bd^2 f_{ck}}$	
	K = 0.078 ≤ K' = 0.167	**Singly Reinforced**
	Since K ≤ K' . Therefore, compression reinforcement is not required.	
	z = d [0.5 + √(0.25 - K/1.134)]	
	z = 421.25 mm	
	0.95d = 432.25 mm	
	z ≤ 0.95d	
	Therefore, use value z.	
	Tension Reinforcement :	
	As = $\frac{M}{0.87 f_{yk} Z}$	
	As = 1004 mm²	
	Provide,	
	5 T 16	**5T16**
	As = 1010 mm²	**As = 1010 mm²**

Project : Seismic Concrete Frame Based on Eurocode for 3-storey		
Ref. / Code	**Calculation**	**Output**
	Checking As min and As max:	
	As min = (0.26 x (fctm) x bd)/fyk	
	where,	
	fctm = 0.3 fck⅔ ; for fck ≤ C50	
	fctm = 2.90	
	So, As min = 260.71 mm²	
	As max = 0.04bh	
	As max = 7000 mm²	
	As min ≤ As provide ≤ As max	**OK**
	Shear Links :	
	Assume cot Θ = 2.5,	
Eq 6.8	$\frac{A_{sw}}{s} = \frac{V_{Ed}}{Z\ f_{yk} \cot \Theta}$	
	= 1.13 mm	
	Provide,	**8mm @ 150 c/c**
	8mm links at 150mm centres, Asw/s = 0.671	**Asw/s = 0.671**
	Minimum link required by EC2:	
	$\frac{A_{sw,min}}{s} = \frac{0.08(\sqrt{f_{ck}})b_w}{f_{yk}}$	
	= 0.333 < 0.671	**OK**
	Deflection:	
	Span-effective depth ratio,	
	$\rho = \frac{100\ A_{s,req}}{bd}$ = 0.63	
Table 7.4N	Basic span-effective depth ratio = 14	
	Modified Ratio, 14 x (As,pro / As,req) = 14.08	
	Span-effective ratio provided, L/d = 13.19	
	< 14.08	**OK**

Project : Seismic Concrete Frame Based on Eurocode for 3-storey

Ref. / Code	Calculation	Output

RC Column Design :

Loading:

Total Ultimate Axial Load taken, N = 611.28 kN

Total Ultimate Moment, M_T = 586.13 kNm

Assume,

Cover	=	25	mm
Bar diameter	=	32	mm
Link diameter	=	12	mm
Column size	=	600 X 600	

d_2/h = 0.91166667

$\frac{N}{bh}$ = 1.698

$\frac{M}{bh^2}$ = 2.714

By using design chart for rectangular column d_2/h = 0.90

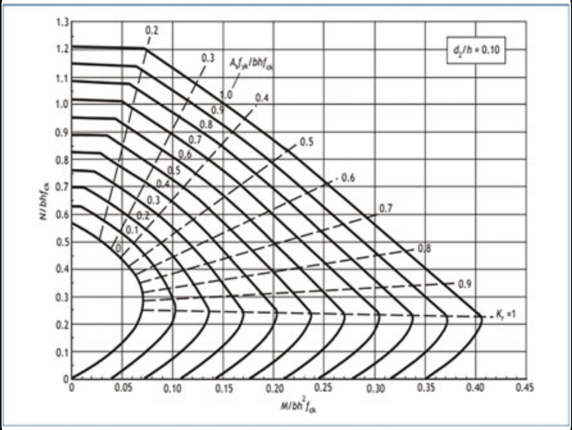

Project : Seismic Concrete Frame Based on Eurocode for 3-storey		
Ref. / Code	**Calculation**	**Output**
	From the design chart :	
	$\frac{100Asc}{bh}$ = 1.5	
	As = 3750 mm²	
	Provide,	
	5 T 32	**5T32**
	As = 4020 mm²	**As = 4020**
	Minimum area of reinforcement :	
	As min = 0.002bh	
	As min = 720 mm²	
	Maximum area of reinforcement :	
	As max = 0.08bh	
	As max = 28800 mm²	
	As min ≤ As provide ≤ As max	**OK**

	UNIVERSITI SAINS MALAYSIA	
	School of Civil Engineering	

Project : Seismic Concrete Frame Design Based on Eurocode for 3-storey

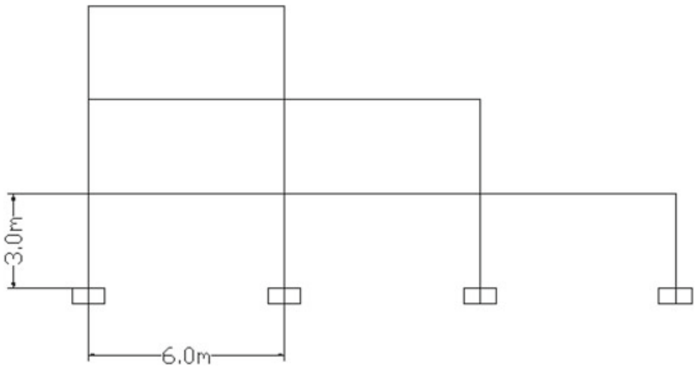

Floor height =	3	m
Bay width =	6	m
Area =	36	m^2

Project : Seismic Concrete Frame Based on Eurocode for 3-storey

Ref. / Code	Calculation	Output
	1st Floor Slab Action Calculation:	
	Dead Load (Gk)	
	(see dead load table below)	
	*Concrete density x thickness (0.15m)	
	Hence, Total Gk = 190.8 kN	
	Live Load (Qk)	
	(see live load table below)	
	Hence, Total Qk = 54 kN	
EC 8 Cl 3.2.4	Combination of the seismic action with other load.	
Eq 3.17	$W_{GQ} = \Sigma G_k \text{ '+' } \Sigma \psi_{Ei} Q_k$	
	where,	
Eq 4.2	$\psi_{Ei} = \varphi . \psi_{2i}$	
Table 4.2	For category A, storeys with correlated occupancies; $\varphi =$ 0.8	
EC 0 Table A1.1	For category A, domestic and residential areas; $\psi_{2i} =$ 0.3	
	Thus, $\psi_{Ei} =$ 0.24	
	Total factored load, W_{GQ} : 203.76 kN	**W_{GQ} = 203.76kN**

Dead Load (DL)	kN/m²
Finishes	1.2
S/w Slab*	3.6
Services	0.5
TOTAL	5.3 x Area (m²)

Live Load (LL)	kN/m²
Imposed load	1.5
TOTAL	1.5 x Area (m²)

Project : Seismic Concrete Frame Based on Eurocode for 3-storey		
Ref. / Code	**Calculation**	**Output**
	Maximum bending moment (approx.) :	
	$M_{GQ} = (WGQ . L) /12$; L = 6m	
	M_{GQ} = 101.88 kNm	**M_{GQ} = 101.88kN**
	Horizontal Seismic Action:	
	Parameters:	
EC 8 Eq 4.6	$T_1 = C_t.H^{3/4}$	
	where,	
	$C_{t\ (Concrete)}$ = 0.075	
Fig. 1(a)	H = 9 m	
	Hence,	
	T_1 = 0.39 s	
Table 3.2	For type 1 elastic response spectra;	
	Ground type : A S : 1 Tb : 0.15s Tc : 0.4s Td : 2s	
	Thus,	
	T_1 in range of Tb and Tc ($Tb \le T1 \le Tc$)	
	Since $Tb \le T1 \le Tc$, use equation 3.15.	
Eq 3.15	Sd(T1) = ag . S . (2.5/q)	
Cl 3.2.1(3)	$a_g = a_{gR} . \gamma_I$	
	where,	
Cl 3.2.1(3)	γI : 1	
Cl 3.2.1(2)	agR : Peak ground acceleration on type A ground* (Assume 0.08g)	
	so, ag = 0.08 g = 0.8 m/s²	

Project : Seismic Concrete Frame Based on Eurocode for 3-storey		
Ref. / Code	**Calculation**	**Output**
Cl 5.2.2.2 Cl5.2.2.2(3)	Behaviour factor (q) q reduced by 20%, but not to be taken as smaller than 1.5 q : 3.2	
Eq 3.15	Sd(T1) = ag . S . (2.5/q) Sd(T1) = 0.63 m/s²	
Cl 4.3.3.2.2	λ = 1	
	For the total mass of the building, *m* m = ∑WGQ.ns which, nb : number of bays ns : number of storeys So, *m* = 1222.56 kN	
	Base Shear Force :	
Cl 4.3.3.2.2	Base shear force, fb Fb = Sd(T1) . *m* . λ Fb = 764.1 kN	**Fb = 764.1 kN**

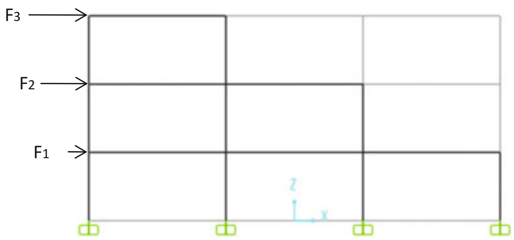

Project : Seismic Concrete Frame Based on Eurocode for 3-storey		
Ref. / Code	**Calculation**	**Output**
	Horizontal sotrey seismic action calculatio:	
Cl 4.3.3.2.2	Distribution of the horizontal seismic force	
	Σzi.mi = (3 x 203.76) + (6 x 203.76) + (9 x 203.76)	
	Σzi.mi = 8557.92	
Cl 4.3.3.2.3(3) Eq 4.11	Fi = Fb . (zi.mi/Σzi.mi)	
	F3 = 491.21 kN F2 = 218.31 kN F1 = 54.58 kN	
	Based on calculation in SAP200,	
	MT = 852.34	
	Wstatic = $1.35G_k + 1.5Q_k$	
	Mstatic = (Wstatic . L) / 12 ; L = 6m	
	Mstatic = 169.29 kNm	**Mstatic = 169.29kNm**
	Thus, M_T = 852.34 ≥ Mstatic	
	M_T ≥ Mstatic	

Project : Seismic Concrete Frame Based on Eurocode for 3-storey		
Ref. / Code	**Calculation**	**Output**
	RC Beam Design :	
	Assume,	
	Bar diameter = 20 mm	
	Link diameter = 10 mm	
	Cover to reinforcement = 25 mm	
	Concrete strength = 30 N/mm²	
	Steel yield stress = 460 N/mm²	
	Beam width = 350 mm	
	Beam depth = 500 mm	
	d = 500 - 25 - 20/2 -10	
	d = 455 mm	
EC2 Cl 6.1	$K = \frac{M}{bd^2 f_{ck}}$	
	K = 0.051 ≤ K' = 0.167	**Singly Reinforced**
	Since K ≤ K' . Therefore, compression reinforcement is not required.	
	z = d [0.5 + √(0.25 - K/1.134)]	
	z = 433.68 mm	
	0.95d = 432.25 mm	
	z ≥ 0.95d	
	Therefore, use value 0.95d	
	Tension Reinforcement :	
	$As = \frac{M}{0.87\ f_{yk}\ 0.95d}$	
	As = 637 mm²	
	Provide,	
	4 T 16	**4T16**
	As = 804 mm²	**As = 804mm²**

Project : Seismic Concrete Frame Based on Eurocode for 3-storey

Ref. / Code	Calculation	Output
	Checking As min and As max:	
	As min = (0.26 x (fctm) x bd)/f_{yk}	
	where,	
	fctm = 0.3 $f_{ck}^{2/3}$; for f_{ck} ≤ C50	
	fctm = 2.90	
	So, As min = 260.71 mm²	
	As max = 0.04bh	
	As max = 7000 mm²	
	As min ≤ As provide ≤ As max	**OK**
	Shear Links :	
	Assume cot Θ = 2.5,	
Eq 6.8	$\frac{A_{sw}}{s} = \frac{V_{Ed}}{Z\, f_{yk} \cot \Theta}$	
	= 0.19 mm	
	Provide, 8mm links at 200mm centres, Asw/s = 0.503	**8mm @ 200 c/c** **Asw/s = 0.503**
	Minimum link required by EC2:	
	$\frac{A_{sw,min}}{s} = \frac{0.08(\sqrt{f_{ck}})b_w}{f_{yk}}$	
	= 0.333 < 0.503	**OK**
	Deflection:	
	Span-effective depth ratio,	
	$\rho = \frac{100\, A_{s,req}}{bd}$ = 0.40	
Table 7.4N	Basic span-effective depth ratio = 14	
	Modified Ratio, 14 x (As,pro / As,req) = 17.68	
	Span-effective ratio provided, L/d = 13.19 < 17.74	**OK**

Project : Seismic Concrete Frame Based on Eurocode for 3-storey

Ref. / Code	Calculation	Output

RC Column Design :

Loading:

Total Ultimate Axial Load taken, N = 305.64 kN

Total Ultimate Moment, MT = 123.00 kNm

Assume,

Cover	=	25	mm
Bar diameter	=	20	mm
Link diameter	=	10	mm
Column size	=	400 X 400	

d_2/h = 0.8875

$\frac{N}{bh}$ = 1.910

$\frac{M}{bh}$ = 1.922

By using design chart for rectangular column d_2/h = 0.10

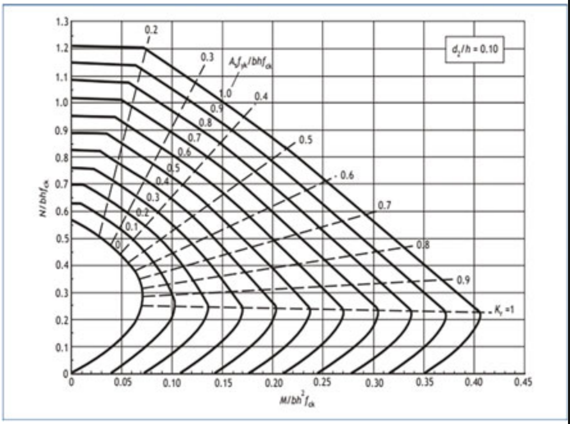

Project : Seismic Concrete Frame Based on Eurocode for 3-storey		
Ref. / Code	**Calculation**	**Output**
	From the design chart :	
	$\frac{A_s f_{yk}}{bhf_{ck}}$ = 0.4	
	As = 640 mm²	
	Provide,	
	3 T 20	**3T20**
	As = 943 mm²	**As = 943mm²**
	Minimum area of reinforcement :	
	As min = 0.002bh	
	As min = 320 mm²	
	Maximum area of reinforcement :	
	As max = 0.08bh	
	As max = 12800 mm²	
	As min ≤ As provide ≤ As max	**OK**

Appendix B
Design of Regular and Irregular Moment-Resisting Steel Frames (MRSF)

F. M. Nazri, *Seismic Fragility Assessment for Buildings due to Earthquake Excitation*, SpringerBriefs in Computational Mechanics,
https://doi.org/10.1007/978-981-10-7125-6

	UNIVERSITI SAINS MALAYSIA	
	School of Civil Engineering	
Project : Seismic Steel Frame Design Based on Eurocode for 3-storey		

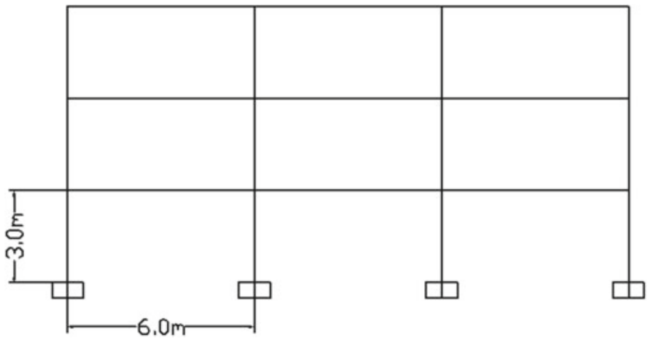

Floor height =	3	m
Bay width =	6	m
Area =	36	m^2

Project : Seismic Steel Frame Based on Eurocode for 3-storey

Ref. / Code	Calculation	Output
	1st Floor Slab Action Calculation:	
	Dead Load (Gk)	

Dead Load (DL)	kN/m²
Finishes	1.2
S/w Slab*	3.6
Services	0.5
TOTAL	5.3 x Area (m²)

*Concrete density x thickness (0.15m)

Hence,

Total Gk = 190.8 kN

Live Load (Qk)

Live Load (LL)	kN/m²
Imposed load	1.5
TOTAL	1.5 x Area (m²)

Hence,

Total Qk = 54 kN

Ref. / Code	Calculation	Output
EC 8 Cl 3.2.4	Combination of the seismic action with other load.	
Eq 3.17	$W_{GQ} = \Sigma G_k \text{ '+' } \Sigma \psi_{Ei} Q_k$	
	where,	
Eq 4.2	$\psi_{Ei} = \varphi . \psi_{2i}$	
Table 4.2	For category A, storeys with correlated occupancies; $\varphi =$ 0.8	
EC 0 Table A1.1	For category A, domestic and residential areas; $\psi_{2i} =$ 0.3	
	Thus, $\psi_{Ei} =$ 0.24	
	Total factored load, W_{GQ} : 203.76 kN	**W_{GQ} = 203.76kN**

Project : Seismic Steel Frame Based on Eurocode for 3-storey		
Ref. / Code	**Calculation**	**Output**
	Maximum bending moment (approx.) :	
	$M_{GQ} = (WGQ \cdot L)/12$; L = 6m	
	$M_{GQ} =$ 101.88 kNm	**M_{GQ} = 101.88kN**
	Horizontal Seismic Action:	
	Parameters:	
EC 8 Eq 4.6	$T_1 = C_t.H^{3/4}$	
	where,	
	$C_{t\ (Concrete)} =$ 0.085	
Fig. 1(a)	H = 9 m	
	Hence,	
	$T_1 =$ 0.44 s	
Table 3.2	For type 1 elastic response spectra;	
	Ground type : A	
	S : 1	
	Tb : 0.15 s	
	Tc : 0.4 s	
	Td : 2 s	
	Thus,	
	T_1 in range of Tc and Td ($Tc \le T1 \le Td$)	
	Since $Tc \le T1 \le Td$, use equation 3.15.	
Eq 3.15	$Sd(T1) = ag \cdot S \cdot (2.5/q) \cdot (Tc/T)$	
Cl 3.2.1(3)	$a_g = a_{gR} \cdot \gamma_I$	
	where,	
Cl 3.2.1(3)	γI : 1	
Cl 3.2.1(2)	agR : Peak ground acceleration on type A ground* (Assume 0.5g)	
	so, ag = 0.08 g = 0.78 m/s²	

Project : Seismic Steel Frame Based on Eurocode for 3-storey		
Ref. / Code	**Calculation**	**Output**
Cl 6.3.2	Behaviour factor (q)	
Table 6.2	q : 4 ; For moment resisting frame (DCM)	
Eq 3.15	Sd(T1) = ag . S . (2.5/q) . (Tc/T)	
	Sd(T1) = 0.44 m/s²	
Cl 4.3.3.2.2	λ = 1	
	For the total mass of the building, *m*	
	m = (WGQ.nb.ns)	
	which, nb : number of bays ns : number of storeys	
	So, *m* = 1833.84 tonne	
	Base Shear Force :	
Cl 4.3.3.2.2	Base shear force, fb	
	Fb = Sd(T1) . *m* . λ	
	Fb = 809.65 kN	**Fb = 809.65 kN**

Project : Seismic Steel Frame Based on Eurocode for 3-storey		
Ref. / Code	**Calculation**	**Output**
	Horizontal sotrey seismic action calculatio:	
Cl 4.3.3.2.2	Distribution of the horizontal seismic force	
	Σzi.mi = (3 x 135.22) + (6 x 135.22) + (9 x 135.22)	
	Σzi.mi = 33009.12	
Cl 4.3.3.2.3(3) Eq 4.11	Fi = Fb . (zi.mi/Σzi.mi)	
	F3 = 404.82 kN	
	F2 = 269.88 kN	
	F1 = 134.94 kN	
	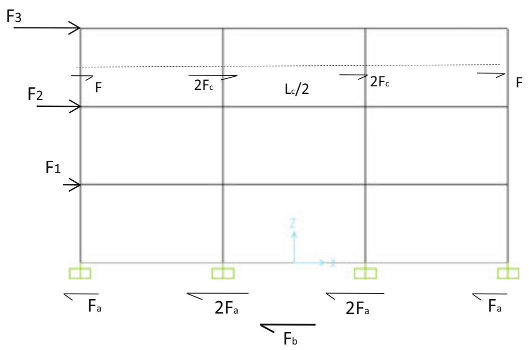	
	Assume, the interrior column is twice as large as exterior column.	
	So,	
	6Fa = Fb	
	Fa = 134.94 kN	
	and	
	6Fc = 134.94 kN	
	Fc = 22.49 kN	

Project : Seismic Steel Frame Based on Eurocode for 3-storey		
Ref. / Code	**Calculation**	**Output**
	Maximum bending moment from sway load :	
	M_E = Fa.Lc + (Fc.Lc/2) ; Lc = 3.0 m	
	M_E = 438.56 kNm	
	Total moment, M_T	
	M_T = $M_E + M_{GQ}$ ≥ Mstatic	
	Wstatic = $1.35G_k + 1.5Q_k$	
	Mstatic = (Wstatic . L) / 12 ; L = 6m	
	Mstatic = 169.29 kNm	**Mstatic = 169.29kNm**
	Thus,	
	M_T = 540.44 ≥ Mstatic	
	M_T ≥ Mstatic	**OK**

Project : Seismic Steel Frame Based on Eurocode for 3-storey		
Ref. / Code	**Calculation**	**Output**
	Steel Beam Design :	
EC3	Required plastic modulus,	
Eq 6.13	$M_{pl,Rd}$ = $W_{pl}.f_y$ for class 1	
	Assume,	
	fy = 275 N/mm²	
	W_{pl} = M/f_y	
	W_{pl} = 369.02 cm³	
	From the section properties, the size beam selected is 254x146x31	
	Properties,	
	W_{pl} = 393 cm³	
	Ix-x = 4410 cm⁴	
	weight of beam = 31.1 kg/m	
	D = 251.4 mm	
	t = 6 mm	
	T = 8.6 mm	
	B = 146.1	
	r = 7.6	
	A = 39.7	
	Thus,	
	$M_{pl,Rd}$ = 108.075 kNm	**Mpl,Rd = 108.075kNm**
	Checking self-weight of beam,	
	Weight of beam = 1.866 kN	
	Factored weight of beam = 1.35 x 4.026kN	
	Factored weight of beam = 2.52 kN	
	Additional moment = (Factored weight of beam x L)/8	
	Additional moment, M_{add} = 1.89 kNm	
	Total moment = 103.35 kNm	
	Total Moment ≤ $M_{pl,Rd}$	**OK**

Project : Seismic Steel Frame Based on Eurocode for 3-storey		
Ref. / Code	**Calculation**	**Output**
	Maximum shear force,	
	Max shear force, V_{ED} = 186 kN	**V_{ED} = 186kN**
	Shear resistance of the section,	
Eq 6.18	$V_{pl,RD} = A_v(f_y/\sqrt{3})$	
	where,	
	A_v = A-2bT+(t+2r)T	
	A_v = 1639.4 mm²	
	Thus,	
	$V_{pl,RD}$ = 260.29 kN	
	$V_{pl,RD}$ > V_{ED}	**OK**
	Deflection checking,	
	$\delta = (WL^3/384EI)$	
	δ = 14.87 mm	**δ = 14.87mm**
	(due to unfactored DL +LL)	
Cl 7.2 Annex A1.4	δ_{max} = span/200	
	δ_{max} = 30 mm	
	$\delta \leq \delta_{max}$	**OK**

Project : Seismic Steel Frame Based on Eurocode for 3-storey		
Ref. / Code	**Calculation**	**Output**
	Steel Column Design :	
	Loading,	
	Total loading applied to column, N_{ed} = 305.64 kN	
	Area, A = $\dfrac{N_{ed}}{f_y}$	
	where,	
	f_y = 275 N/mm²	
	so,	
	Area, A = 11.11 cm²	
	From the section properties, the size column selected is 203x203x86	
	Properties,	
	Area of section, A = 110 cm²	
	Depth od section, D = 222.2 mm	
	Width of section, B = 209.1 mm	
	Thickness of flange,T = 20.5 mm	
	Thickness of web,t = 12.7 mm	
	Root radius, r = 10.2 mm	
	Plastic modulus, Sy = 977 cm³	
	Radius of gyration, rx = 9.28 cm	
	Radius of gyration, ry = 5.34 cm	
	Section classification,	
	Flange :	
Table 5.2	ε = 0.92	
	For bending = 72ε = 66.24	
	For compression = 33ε = 30.36	
	Depth of cross section,c = D - 2T-2r = 160.8 mm	
	for class 1,	
	c/t = 12.66 ≤ 72ε	**Class 1**
	≤ 33ε	**Class 1**
	Therefore, the flange is class 1.	

Project : Seismic Steel Frame Based on Eurocode for 3-storey		
Ref. / Code	**Calculation**	**Output**
	Web :	
	ε = 0.92	
	For compression = 9ε = 8.28	
	Depth of cross section,c = B/2 -r = 94	
	for class1,	
	c/t = 7.43 ≤ 9ε	**Class 1**
	Therefore, the web is class 1. Thus, the whole section is class 1.	
	Maximum shear force,	
	V_{ED} = 161.63 kN	
	Shear resistance of the section,	
Eq 6.18	$V_{pl,RD} = A_v(f_y/\sqrt{3})$	
	where,	
	A_v = A-2btT+(t+2r)T	
	A_v = 3105.45 mm²	
	so,	
	$V_{pl,RD}$ = 569.33 kN	
	$V_{pl,RD}$ > V_{ED}	
Cl 6.2.3 (2)	Resistance of cross section,	
Eq 6.6	$N_{pl.Rd}$ = A.f_y 3025 kN	
	Moment resistance,	
	Moment design, M_{ED} = 103.35 kNm	
	For class 1,	
	$W_{pl,y}$ = 977000 mm³	
	So,	
	$M_{c,Rd}$ = 268.675 kNm > M_{ED}	**OK**

Project :	Seismic Steel Frame Based on Eurocode for 3-storey	
Ref. / Code	**Calculation**	**Output**
	Bending and axial compression,	
	Slenderness for flexural buckling.	
Eq 6.50	$\lambda_{bar} = L/(i_{x\text{-}x}.\lambda_l)$ for class 1.	
	where,	
	$\lambda_l =$ 93.9ε = 86.39	
	so,	
	$\lambda_{bar} =$ 1.30	
Fig. 6.4	Hence reduction factor = 0.44	
Eq 6.55	$M_{b,Rd} = \chi_{LT}.W_y.f_y$	
	where,	
	$M_{b,Rd} =$ 1331 kN	
	Combination of axial and bending,	
	Simplified equation in EC3.	
	$(M_{ED}/M_{c,Rd}) < 1$	
	$0.38 < 1$	**OK**
	$(NEd/Mb,Rd) < 1$	
	$0.23 < 1$	**OK**

	UNIVERSITI SAINS MALAYSIA	
	School of Civil Engineering	
Project : Seismic Steel Frame Design Based on Eurocode for 3-storey		

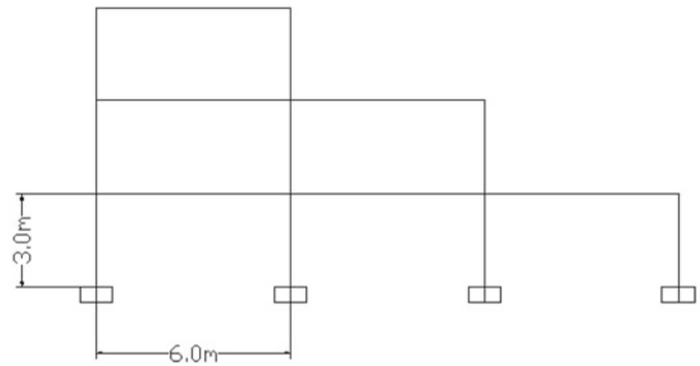

Floor height =	3	m
Bay width =	6	m
Area =	36	m^2

Project : Seismic Steel Frame Based on Eurocode for 3-storey

Ref. / Code	Calculation	Output
	1st Floor Slab Action Calculation:	
	Dead Load (Gk)	

Dead Load (DL)	kN/m²
Finishes	1.2
S/w Slab*	3.6
Services	0.5
TOTAL	5.3

x Area (m²)

*Concrete density x thickness (0.15m)

Hence,

Total Gk = 190.8 kN

Live Load (Qk)

Live Load (LL)	kN/m²
Imposed load	1.5
TOTAL	1.5

x Area (m²)

Hence,

Total Qk = 54 kN

Ref. / Code	Calculation	Output
EC 8 Cl 3.2.4	Combination of the seismic action with other load.	
Eq 3.17	$W_{GQ} = \Sigma G_k$ '+' $\Sigma \psi_{Ei} Q_k$	
	where,	
Eq 4.2	$\psi_{Ei} = \varphi . \psi_{2i}$	
Table 4.2	For category A, storeys with correlated occupancies; φ = 0.8	
EC 0 Table A1.1	For category A, domestic and residential areas; ψ_{2i} = 0.3	
	Thus, ψ_{Ei} = 0.24	
	Total factored load, W_{GQ} : 203.76 kN	**W_{GQ} = 203.76kN**

Project : Seismic Steel Frame Based on Eurocode for 3-storey

Ref. / Code	Calculation	Output
	Maximum bending moment (approx.) :	
	$M_{GQ} = (WGQ . L) /12$; L = 6m	
	$M_{GQ} =$ 101.88 kNm	**M_{GQ} = 101.88kN**
	Horizontal Seismic Action:	
	Parameters:	
EC 8		
Eq 4.6	$T_1 = C_t.H^{3/4}$	
	where,	
	$C_{t\,(steel)} =$ 0.085	
Fig. 1(a)	H = 9 m	
	Hence,	
	$T_1 =$ 0.44 s	
Table 3.2	For type 1 elastic response spectra;	
	Ground type : A	
	S : 1	
	Tb : 0.15 s	
	Tc : 0.4 s	
	Td : 2 s	
	Thus,	
	T_1 in range of Tc and Td $(Tc \le T1 \le Td)$	
	Since $Tc \le T1 \le Td$, use equation 3.15.	
Eq 3.15	$Sd(T1) = ag . S . (2.5/q) . (Tc/T)$	
Cl 3.2.1(3)	$a_g = a_{gR}. \gamma_I$	
	where,	
Cl 3.2.1(3)	γI : 1	
Cl 3.2.1(2)	agR : Peak ground acceleration on type A ground* (Assume 0.5g)	
	so, ag = 0.08 g = 0.78 m/s²	

Project : Seismic Steel Frame Based on Eurocode for 3-storey		
Ref. / Code	**Calculation**	**Output**
Cl 6.3.2	Behaviour factor (q)	
Cl 6.3.2(2)	q should be reduced by 20% for non-regular in elevation	
	q : 3.2 ; For moment resisting frame (DCM)	
Eq 3.15	Sd(T1) = ag . S . (2.5/q) . (Tc/T)	
	Sd(T1) = 0.55 m/s^2	
Cl 4.3.3.2.2	λ = 1	
	For the total mass of the building, *m*	
	m = (WGQ.nb.ns)	
	which,	
	nb : number of bays	
	ns : number of storeys	
	So,	
	m = 1222.56 kN	
	Base Shear Force :	
Cl 4.3.3.2.2	Base shear force, fb	
	Fb = Sd(T1) . *m* . λ	
	Fb = 674.71 kN	**Fb = 674.71 kN**

Project : Seismic Steel Frame Based on Eurocode for 3-storey		
Ref. / Code	**Calculation**	**Output**
	Horizontal sotrey seismic action calculatio:	
Cl 4.3.3.2.2	Distribution of the horizontal seismic force	
Cl 4.3.3.2.3(3) Eq 4.11	Fi = Fb . (zi.mi/Σzi.mi)	
	F3 = 433.74 kN F2 = 192.77 kN F1 = 48.19 kN	

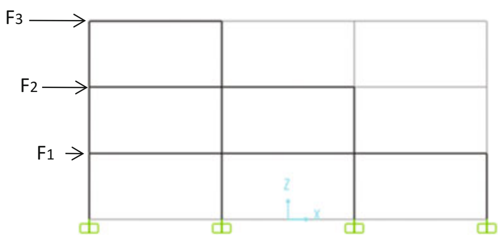

Project : Seismic Steel Frame Based on Eurocode for 3-storey		
Ref. / Code	**Calculation**	**Output**
	Based on calculation in SAP200, MT = 475.97 Wstatic = $1.35G_k + 1.5Q_k$ Mstatic = (Wstatic . L) / 12 ; L = 6m Mstatic = 169.29 kNm	**Mstatic = 169.29kNm**
	Thus, M_T = 475.97 ≥ Mstatic M_T ≥ Mstatic	**OK**

Project : Seismic Steel Frame Based on Eurocode for 3-storey		
Ref. / Code	**Calculation**	**Output**
	Steel Beam Design :	
EC3	Required plastic modulus,	
Eq 6.13	$M_{pl,Rd}$ = $W_{pl}.f_y$ for class 1	
	Assume,	
	f_y = 275 N/mm²	
	W_{pl} = M/f_y	
	W_{pl} = 400.40 cm³	
	From the section properties, the size beam selected is 254x146x37	
	Properties,	
	W_{pl} = 483 cm³	
	Ix-x = 5540 cm⁴	
	weight of beam = 37 kg/m	
	D = 256 mm	
	t = 6.3 mm	
	T = 10.9 mm	
	B = 101.6	
	r = 7.6	
	A = 47.2	
	Thus,	
	$M_{pl,Rd}$ = 132.825 kNm	**Mpl,Rd = 132.83kNm**
	Checking self-weight of beam,	
	Weight of beam = 2.22 kN	
	Factored weight of beam = 1.35 x 4.026kN	
	Factored weight of beam = 3.00 kN	
	Additional moment = (Factored weight of beam x L)/8	
	Additional moment, M_{add} = 2.25 kNm	
	Total moment = 112.36 kNm	
	Total Moment ≤ $M_{pl,Rd}$	**OK**

Project : Seismic Steel Frame Based on Eurocode for 3-storey		
Ref. / Code	**Calculation**	**Output**
	Maximum shear force,	
	Max shear force, V_{ED} = 189.95 kN	**V_{ED} = 189.95kN**
	Shear resistance of the section,	
Eq 6.18	$V_{pl,RD} = A_v(f_y/\sqrt{3})$	
	where,	
	A_v = A-2bT+(t+2r)T	
	A_v = 2739.47 mm²	
	Thus,	
	$V_{pl,RD}$ = 434.95 kN	
	$V_{pl,RD}$ > V_{ED}	**OK**
	Deflection checking,	
	$\delta = (WL^3/384EI)$	
	δ = 11.84 mm	**δ = 11.84mm**
	(due to unfactored DL +LL)	
Cl 7.2 Annex A1.4	δ_{max} = span/200	
	δ_{max} = 30 mm	
	$\delta \le \delta_{max}$	**OK**

Project : Seismic Steel Frame Based on Eurocode for 3-storey		
Ref. / Code	**Calculation**	**Output**
	Steel Column Design :	
	Loading,	
	Total loading applied to column, N_{ed} = 305.64 kN	
	Area, A = $\frac{N_{ed}}{f_y}$	
	where, f_y = 275 N/mm²	
	so, Area, A = 11.11 cm²	
	From the section properties, the size column selected is 203x203x86	
	Properties,	
	Area of section, A = 110 cm²	
	Depth od section, D = 222.2 mm	
	Width of section, B = 209.1 mm	
	Thickness of flange,T = 20.5 mm	
	Thickness of web,t = 12.7 mm	
	Root radius, r = 10.2 mm	
	Plastic modulus, Sy = 977 cm³	
	Radius of gyration, rx = 9.28 cm	
	Radius of gyration, ry = 5.34 cm	
	Section classification,	
	Flange :	
Table 5.2	ε = 0.92	
	For bending = 72ε = 66.24	
	For compression = 33ε = 30.36	
	Depth of cross section,c = D - 2T-2r = 160.8 mm	
	for class 1,	
	c/t = 12.66 ≤ 72ε	**Class 1**
	≤ 33ε	**Class 1**
	Therefore, the flange is class 1.	

Project : Seismic Steel Frame Based on Eurocode for 3-storey		
Ref. / Code	**Calculation**	**Output**
	Web :	
	$\varepsilon =$ 0.92	
	For compression = $9\varepsilon =$ 8.28	
	Depth of cross section,c = $B/2 - r =$ 94	
	for class1,	
	$c/t =$ 7.43 $\leq$ 9ε	**Class 1**
	Therefore, the web is class 1. Thus, the whole section is class 1.	
	Maximum shear force,	
	$V_{ED} =$ 161.55 kN	
	Shear resistance of the section,	
Eq 6.18	$V_{pl,RD} = A_v(f_y/\sqrt{3})$	
	where,	
	$A_v = A-2btT+(t+2r)T$	
	$A_v =$ 3105.45 mm^2	
	so,	
	$V_{pl,RD} =$ 569.33 kN	
	$V_{pl,RD} > V_{ED}$	**OK**
Cl 6.2.3 (2)	Resistance of cross section,	
Eq 6.6	$N_{pl.Rd} = A.f_y$ 3025 kN	
	Moment resistance,	
	Moment design, $M_{ED} =$ 112.36 kNm	
	For class 1,	
	$W_{pl,y} =$ 977000 mm^3	
	So,	
	$M_{c,Rd} =$ 268.675 kNm $> M_{ED}$	**OK**

Project : Seismic Steel Frame Based on Eurocode for 3-storey		
Ref. / Code	**Calculation**	**Output**
	Bending and axial compression,	
	Slenderness for flexural buckling.	
Eq 6.50	$\lambda_{bar} = L/(i_{x-x}.\lambda_l)$ for class 1.	
	where,	
	$\lambda_l = 93.9\varepsilon = 86.39$	
	so,	
	$\lambda_{bar} = 1.30$	
Fig. 6.4	Hence reduction factor = 0.44	
Eq 6.55	$M_{b,Rd} = \chi_{LT}.W_y.f_y$	
	where,	
	$M_{b,Rd} =$ 1331 kN	
	Combination of axial and bending,	
	Simplified equation in EC3.	
	$(M_{ED}/M_{c,Rd}) < 1$	
	$0.42 < 1$	**OK**
	$(NEd/Mb,Rd) < 1$	
	$0.23 < 1$	**OK**

Bibliography

ATC, A. 1996. 40, Seismic evaluation and retrofit of concrete buildings. Applied Technology Council, report ATC-40. Redwood City.

Bai, J.-W., P. Gardoni, and M.B.D. Hueste. 2011. Story-specific demand models and seismic fragility estimates for multi-story buildings. *Structural Safety* 33 (1): 96–107.

Chintanapakdee, C., and A.K. Chopra. 2004. Seismic response of vertically irregular frames: response history and modal pushover analyses. *Journal of Structural Engineering* 130 (8): 1177–1185.

Defallah, H.M.R. 2010. Influence of Excitation Angles of Ground Motion with Forward Directivity Effect on the Response of Regular and Symmetric Reinforced Concrete Buildings, Universiti Sains Malaysia.

Doksil, M. 2015. Sabah quake caused by friction between tectonic plates. The Borneo Post: 4.

EN, B. 2005. 1998. 2 Eurocode 8–design of structure for earthquake resistance.

Faisal, A., T.A. Majid, and G.D. Hatzigeorgiou. 2013. Investigation of story ductility demands of inelastic concrete frames subjected to repeated earthquakes. *Soil Dynamics and Earthquake Engineering* 44: 42–53.

Fazli, H., and T.A. Majid. 2013. Seismic Performance of 3 Storey Irregular Reinforced Concrete (RC) Frames Under Repeated Earthquakes. *Caspian Journal of Applied Science Research* 2: 60–65.

FEMA-356. 2000. Prestandard and Commentary for the Seismic Rehabilitation of Buildings: FEMA-356, Federal Emergency Management Agency Washington.

Hatzigeorgiou, G. 2010. Behavior factors for nonlinear structures subjected to multiple near-fault earthquakes. *Computers & Structures* 88 (5): 309–321.

Hatzigeorgiou, G.D., and D.E. Beskos. 2009. Inelastic displacement ratios for SDOF structures subjected to repeated earthquakes. *Engineering Structures* 31 (11): 2744–2755.

Hatzigeorgiou, G.D., and A.A. Liolios. 2010. Nonlinear behaviour of RC frames under repeated strong ground motions. *Soil Dynamics and Earthquake Engineering* 30 (10): 1010–1025.

Hatzivassiliou, M., and G.D. Hatzigeorgiou. 2015. Seismic sequence effects on three-dimensional reinforced concrete buildings. *Soil Dynamics and Earthquake Engineering* 72: 77–88.

Humar, J., and E. Wright. 1977. Earthquake response of steel-framed multistorey buildings with set-backs. *Earthquake Engineering & Structural Dynamics* 5 (1): 15–39.

Hwang, H.H., and J.-R. Huo. 1994. Generation of hazard-consistent fragility curves. *Soil Dynamics and Earthquake Engineering* 13 (5): 345–354.

Kumar, C.R., K.B. Narayan, and R. Venkat. 2014. Methodology for Probabilistic Seismic Risk Evaluation of Building Structure Based on Pushover Analysis.

Modakwar, N.P., S.S. Meshram, and D.W. Gawatre. 2014. Seismic Analysis of Structures with Irregularities. InInternational Conference on Advances in Engineering and Technology, IOSR Journal of Mechanical and Civil Engineering.

Najafi, L.H., and M. Tehranizadeh. 2015. Ground Motion Selection and Scaling in Practice. Periodica Polytechnica Civil Engineering.

F. M. Nazri, *Seismic Fragility Assessment for Buildings due to Earthquake Excitation*, SpringerBriefs in Computational Mechanics,
https://doi.org/10.1007/978-981-10-7125-6

Nazri, F.M., and Y.K. Pang. 2014. Seismic Performance of Moment Resisting Steel Frame Subjected to Earthquake Excitations. *Frontiers of Structural and Civil Engineering* 8, no. 1: 19–25.

Soni, D.P., and B.B. Mistry. 2006. Qualitative review of seismic response of vertically irregular building frames. *ISET Journal of Earthquake Technology, Technical Note* 43 (4): 121–132.

Varadharajan, S., V. Sehgal, and B. Saini. 2015. Fundamental time period of RC Setback Buildings. *Concrete Research Letters* 5 (4): 901–935.

Zaini, S.S., S. Sawada, and H. Goto. 2012. Proposal for Seismic Resistant Design in Malaysia: Assessment of Possible Ground Motions in Peninsular Malaysia. *Disaster Prevention Research Institute Annuals* 55: 81–94.

Zulham, M., A. Bin, M. Zahid, T.A. Majid, and A. Faisal. 2012. Effect Of Repeated Near Field Earthquake to the High-Rise Rc Building.

Index

F. M. Nazri, *Seismic Fragility Assessment for Buildings due to Earthquake Excitation*, SpringerBriefs in Computational Mechanics,
https://doi.org/10.1007/978-981-10-7125-6